British Geological Survey

NATURAL ENVIRONMENT RESEARCH COUNCIL

Onshore Carboniferous Basins- third review report

Energy Systems & Basin Analysis Programme

Internal Report CR/16/139

BRITISH GEOLOGICAL SURVEY

Onshore Carboniferous Basins- third review report

E Hough, K Bateman, RJ Cuss, JF Harrington, RB Haslam, JA Hennissen, PRN Hobbs, AD Kilpatrick, V Moss-Hayes, G Purser, L Selby, CH Vane, CN Waters

Maps and diagrams in this book use topography based on Ordnance Survey mapping.

Keyworth, Nottingham   British Geological Survey   2016

BRITISH GEOLOGICAL SURVEY

The full range of our publications is available from BGS shops at Nottingham, Edinburgh, London and Cardiff (Welsh publications only) see contact details below or shop online at www.geologyshop.com

The London Information Office also maintains a reference collection of BGS publications, including maps, for consultation.

We publish an annual catalogue of our maps and other publications; this catalogue is available online or from any of the BGS shops.

The British Geological Survey carries out the geological survey of Great Britain and Northern Ireland (the latter as an agency service for the government of Northern Ireland), and of the surrounding continental shelf, as well as basic research projects. It also undertakes programmes of technical aid in geology in developing countries.

The British Geological Survey is a component body of the Natural Environment Research Council.

British Geological Survey offices

BGS Central Enquiries Desk

Tel 0115 936 3143   Fax 0115 936 3276
email enquiries@bgs.ac.uk

Environmental Science Centre, Keyworth, Nottingham NG12 5GG

Tel 0115 936 3241   Fax 0115 936 3488
email sales@bgs.ac.uk

The Lyell Centre, Research Avenue South, Edinburgh EH14 4AP

Tel 0131 667 1000   Fax 0131 668 2683
email scotsales@bgs.ac.uk

Natural History Museum, Cromwell Road, London SW7 5BD

Tel 020 7589 4090   Fax 020 7584 8270
Tel 020 7942 5344/45   email bgslondon@bgs.ac.uk

Columbus House, Greenmeadow Springs, Tongwynlais, Cardiff CF15 7NE

Tel 029 2052 1962   Fax 029 2052 1963

Maclean Building, Crowmarsh Gifford, Wallingford OX10 8BB

Tel 01491 838800   Fax 01491 692345

Geological Survey of Northern Ireland, Department of Enterprise, Trade & Investment, Dundonald House, Upper Newtownards Road, Ballymiscaw, Belfast, BT4 3SB

Tel 028 9038 8462   Fax 028 9038 8461

www.bgs.ac.uk/gsni/

Parent Body

Natural Environment Research Council, Polaris House, North Star Avenue, Swindon SN2 1EU

Tel 01793 411500   Fax 01793 411501
www.nerc.ac.uk

Website www.bgs.ac.uk
Shop online at www.geologyshop.com

Contents

FIGURES

TABLES

Summary

Following amalgamation of work packages 1 and 2, activities of the Onshore Carboniferous Basins research consortium are split into 3 main work packages.

A brief review of main achievements is:

Work Package 1: Basin analysis and tectonostratigraphy; characterisation of shale depositional facies

Analysis and modelling of age-equivalent units in progress- facies predictive model extended to complete Bowland-Hodder area, with addition of borehole facies data in progress;

Clean dataset of previously published organic geochemistry results for BGS-curated core, cuttings and samples;

Targeted fieldwork survey complete (River Noe, Edale, Derbyshire).

Thin sections prepared from 5 boreholes, in order to understand the relationship between organic matter, mineralogy and microfacies, and diagenetic processes;

Future options:

Progress analysis and modelling of age-equivalent units across Bowland-Hodder subcrop;

Progress database of unpublished biostratigraphical and analytical (Rock Eval; X-ray diffraction) data held by BGS of Bowland-Hodder unit;

Develop palaeofacies maps;

Develop predictive models.

Work package 3: Development of chemical stratigraphies through prospective parts of the stratigraphic column

Outcrop samples (26) run for RockEval and mineral XRD;

Newly published IFPEN shale play method provides an enhanced understanding of free, sorbed and bound hydrocarbons.

Future options:

To fully interpret and integrate results of Rock Eval/TOC, X-ray diffraction and facies to understand any linkages between depositional facies and geochemistry;

Understand shale maturity indices from clay mineralogy;

Link mineralogy to a likely brittleness index.

Work Package 4: Hydromechanical behaviour of shales

Point Load Strength Index (converted to Unconfined Strength)/strength anisotropy interpreted for samples from Crimple Beck and Cow Ark 7 boreholes;

FRACKiT test used to give indirect tensile strength data; problems with sample material give doubts in relating results to tensile strength;

Progress of lab based hydrofracture studies, analogue hydrofracture studies dependant on production of modified apparatus;

Water uptake study indicates shale acts as a semi-permeable membrane allowing osmosis of water into shale.

Future options:

Investigate relationship between Point Load Strength Index (PLSI), Uniaxial Compressive Strength (UCS) and Indirect Tensile Strength (ITS).

1 Introduction

The BGS is co-ordinating the Onshore Carboniferous Basins research consortium, which is focussed on achieving a better understanding of the Bowland Shale in northern England. The broad aim is to understand the geological variability of the formation from a basin- through to micro-scale, and assess the impact of variability on hydrocarbon generation, storage and production (for example, the co-incidence or otherwise of factors including organic content and kerogen type; mineralogy; and engineering behaviour).

This report is the third summary report describing activities of the consortium, covering the period October 2015 – June 2016. A series of 3 inter-related work packages are designed to improve understanding of the Bowland Shale of northern England. The original numbering of these is retained to allow continuity between previous progress reports. Specifically, these work packages address:

1. Work Package 1,2: Basin analysis of the Pennine Basin; Characterization of shale facies;
2. Work Package 3: Development of chemical stratigraphies through prospective parts of the stratigraphic column;
3. Work Package 4: Hydromechanical behaviour of shales.

Two work packages outside the consortium are also considered, namely

4. Retrieval of new materials to test
5. Reprocessing of 3D seismic data to assess rock properties

Descriptions of previous activities have been released, covering the period July 2014 to March 2015 (Hough et al., 2015a), and the period April 2015 to September 2015 (Hough et al., 2015b).

The consortium currently has 4 sponsors who each contribute £25 000 per year; BGS contributes around £200 000 annually, which results in an annual budget of approximately £300 000. The consortium is planned to last 3 years initially, and started in July 2014 with a scheduled end date of June 2017.

2 Consortium administration

2.1 FINANCE

Presently there are 4 sponsors to the consortium, each subscribing £25 000 per annum for 3 years. The schedule of invoicing is given in Table 1.

2.2 COMMUNICATION

A webpage publicising the Onshore Carboniferous Basins consortium is at http://www.bgs.ac.uk/research/energy/onshoreCarboniferousBasins.html

2.3   MEETING DATES

The next consortium progress meeting is scheduled for February 2017; with one meeting anticipated in June 2017 and one further meeting to follow by November 2017.

Table 1. Schedule of fee payment and progress/review meeting dates.

Sponsor	Jul-14	Aug-14	Sep-14	Oct-14	Nov-14	Dec-14	Jan-15	Feb-15	Mar-15	Apr-15	May-15	Jun-15	Jul-15	Aug-15	Sep-15	Oct-15	Nov-15	Dec-15	Jan-16	Feb-16	Mar-16	Apr-16	May-16	Jun-16	Jul-16	Aug-16	Sep-16	Oct-16	Nov-16	Dec-16	Jan-17	Feb-17	Mar-17	Apr-17	May-17	Jun-17
	Year 1 July 2014 - June 2015												Year 2 July 2015 - June 2016												Year 3 July 2016 - June 2017											
Centrica										25 k			25 k												25 k											
DECC								75 k																												
Engie										25 k			25 k												25 k											
Total										25 k			25 k												25 k											

Invoice date	
Meeting date	

3 Work Packages 1, 2: Basin analysis and facies analysis of the Pennine Basin, and associated data

The BGS holds a large dataset referencing the stratigraphical marker horizons within the Bowland Shale, from across the Pennine Basin. Much of this data was generated during field mapping campaigns and assessments of the deep geological structure of the UK. Whilst some of this data has been published (for example, as figures in Geological Memoirs), much remains unpublished as notations on borehole logs, interpreted down-hole logs, and descriptions in unpublished field-map descriptions. This data has been collated and databased in the BGS corporate 'Borehole Geology' database. Additionally, lithostratigraphical and chronostratigraphical marker horizons have been extracted from published reports, maps and boreholes for which BGS hold Bowland Shale core materials, and entered into BGS corporate databases (Borehole Geology and the Stratigraphic Surfaces Database). Where there is enough information available, broad depositional and/or diagenetic facies have been assigned to stratigraphic intervals, allowing a first-pass at basin-fill modelling to be undertaken. This databasing exercise has been completed for the Pennine Basin area, and provides a dataset from which a structural model can be developed, and modelling of the basin can proceed.

3.1 BASIN ANALYSIS

The development of an initial structural model has focussed in north-west England, where bio-stratigraphical and litho-stratigraphical data are richest. The structural model will be extended in the next phase of work to include the whole area covered by the BGS-DECC Bowland-Hodder assessment area of Andrews (2013). However, due to the large area being modelled and the paucity of data, the resolution of the model will be reduced significantly to enable successful modelling of relatively thin units over large areas of ground.

3.1.1 Data sources

The development of a tectonstratigraphic model for the onshore Carboniferous basins utilises:
1. litho-stratigraphic down-hole database with chronostratigraphy mapped onto the lithostratigraphic units. This currently numbers 251 entries. This includes data originally interpreted from the BGS Stratigraphic Surfaces database, BGS Borehole Geology database and new interpretations based on boreholes and data not previously databased (e.g., from unpublished data held by BGS).
2. 1:50 000-scale mapped outcrop data, including identified marine band horizons
3. 1:625 000-scale generalised map boundaries
4. Subsurface memoir surfaces
5. Field exposure logs
6. DECC shale gas report surfaces
7. UK3D deep cross-section lines

3.1.2 Modelling methodology

The modelling workflow followed the standard BGS modelling methodology (e.g., Monaghan & Pouliquen, 2009) as outlined in Figure 1. The principal phases of the workflow are firstly the development of a network of fault planes and secondly a series of stratigraphic surfaces. These planar features delimit volumes through which rock properties and facies can be interpolated or simulated. The modelling has been carried out using GOCAD-SKUA, which accommodates data derived from BGS corporate databases, and allows time-equivalent surfaces to be mapped out regionally. Geocellular models can be derived from the structural model and properties and facies interpolated throughout the volume.
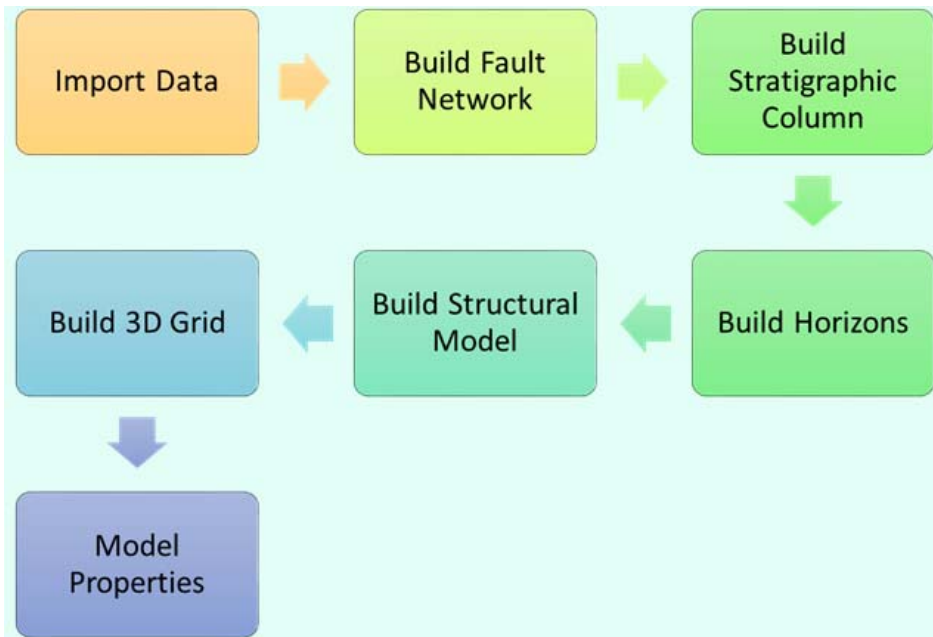
Figure 1 GOCAD-SKUA structural modelling workflow

The initial region selected for modelling has the densest concentration of of borehole data and field mapped locations in which key marker horizons have been identified (Figure 2). The region covers area of 94,600km^2.
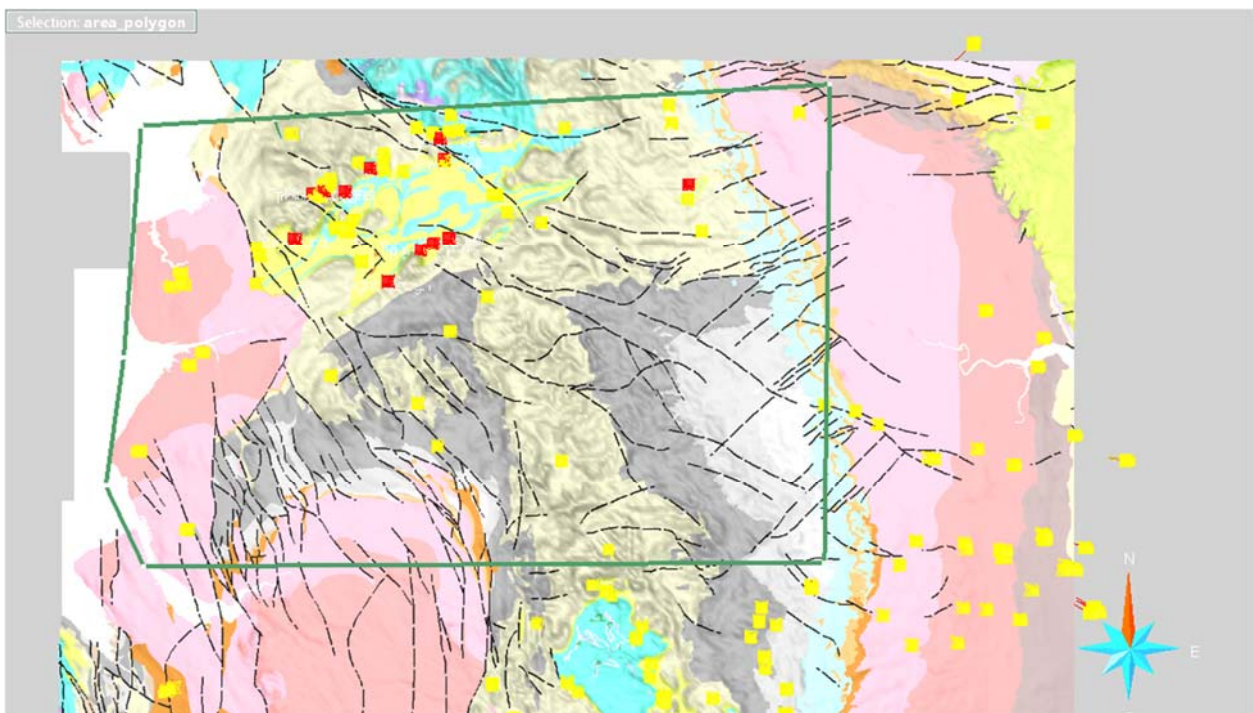
Figure 2 Area modelled (green polygon), well distribution (yellow rigs) and surface logs (red rigs).

For this study, stratigraphic modelling has relied on marine-band marker horizons identified in boreholes, which have been databased in the BGS corporate 'Borehole Geology' database, and at outcrop where they have been extracted from digital maps and linework. The following markers

4

have been identified and the bases of stratigraphic units (unless otherwise stated) imported along well paths: Carboniferous Limestone (Top); the following Marine Bands: B2; H2; H1; P1; P2; E1; E2; R1; R2; G1; base Westphalian A; Base Permo-Trias. Although all the markers were coded not all horizons were modelled due to scale of the model (covering a large area and the thickness between markers can be quite small and therefore creates artefacts in the modelling workflow). Additionally some horizons are identified by a relatively small number of occurrences in boreholes and at outcrop, with poor spatial coverage across the region. All surfaces are tied to the well markers during the modelling process.

The fault network was derived principally from the DECC shale gas study (Andrews, 2013), with additional faults added where they could be identified, with the fault network altered where there was discrepancy between closely-spaced borehole markers and large deflections on modelled surfaces. For simplicity and in order to ensure consistency across the model, all faults were modelled as vertical faults. This simplification has a minor effect on the model due to the high angle of most faults in the region and due to the lack of structural information on the fault network (Dip and throw).

The principal modelled surfaces were primarily based on chrono-stratigraphical marker horizons as the litho-stratigraphy across the region varies and is not directly comparable between basins. Locally, Litho-stratigraphical surfaces were modelled below and above the Bowland Shale interval, with the following stratigraphic picks interpreted where possible (Figure 3):
- P1 (intra-Asbian: Goniatites crenistria Marine Band)
- P2 (intra-Brigantian: Lusitanoceras granosus Marine Band)
- E1 (Base Namurian: Cravenoceras leion Marine Band)
- E2 (Base Arnsbergian: Cravenoceras cowlingense Marine Band)
- H1 (Base Chokerian: Isohomoceras subglobosum Marine Band)
- R1 (Baae Kinderscoutian: Hodsonites magistrorum) Marine Band
- R2 (Base Marsdenian: Bilinguites gracilis Marine Band)
- G1 (Base Yeadonian: Cancelloceras cancellatum Marine Band)
- Base Coal Measures
- Base Permo-Triassic
- Topography

In addition to the chronostratigraphic horizons identified from boreholes and surface exposure, surfaces for the Base Namurian, Base Coal Measures and Permian-Triassic Unconformity were also imported from the published UK3D dataset (http://www.bgs.ac.uk/research/ukgeology/nationalGeologicalModel/GB3D.html), and the Craven Basin BGS subsurface memoir (Kirby et al., 2000).
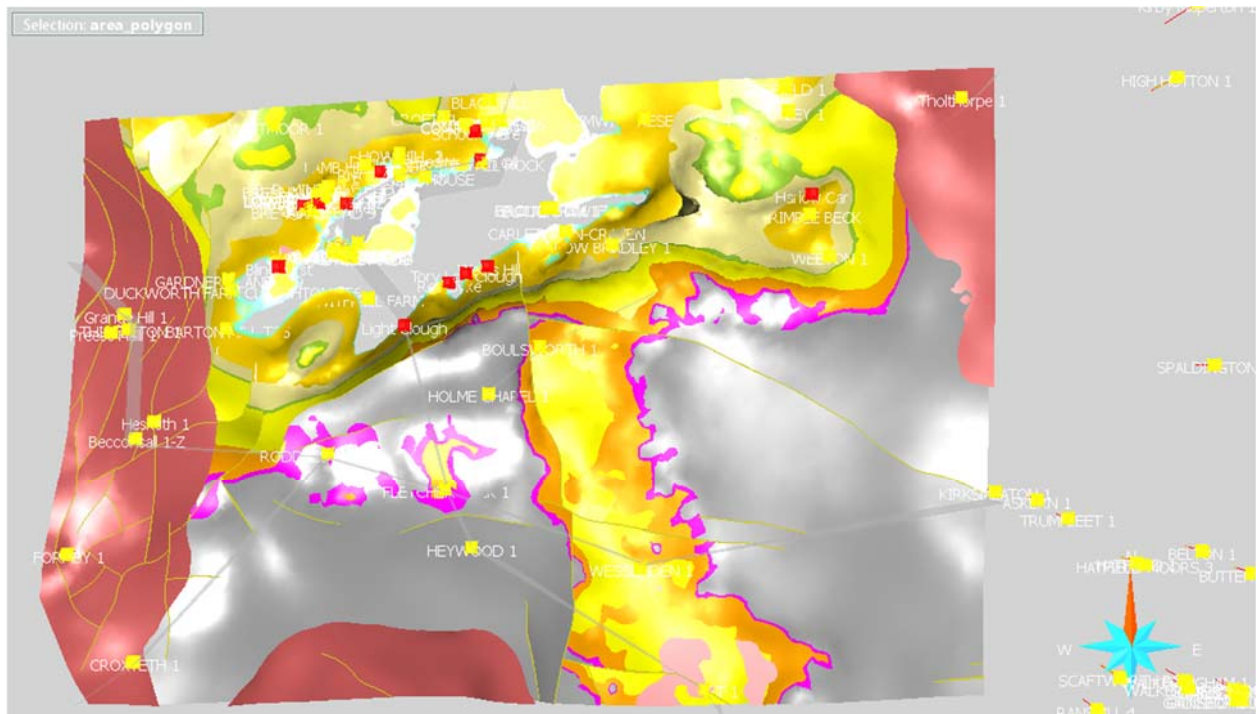
Figure 3 Modelled surfaces

Based on the mapped surfaces, a volumetric geocelluar model was built for all units between the Carboniferous Limestone and the Base Coalmeasures and Permian unconformity. The geocellular model consists of a grid 1,162,996 cells.

Where the data in well logs is of sufficient detail, it has been possible to apply a gross facies to the down-hole information, based on the key facies identified during outcrop logging and reported in the first and second report. These are:

- Mudstone (MDST)
- Organic rich mudstone(OMDST)
- Calcareous mudstone (CMDST)
- Ironstone Mudstone (IMDST)
- Sandstone (including siltstone; SDST)
- Limestone (LST)

The logs were imported into GoCAD and the facies upscaled to the geocellular model. As there is a natural bias in the logs towards mudstone and sandstone with these units being typically thicker, the mid-point for each facies was used instead of the maximum or average and this addresses the potential for under-representation of the subordinate facies in the model. Stochastic methods are often more difficult to interpret by geologists and therefore an interpolation of facies through the rock volume has been used. The interpolation is guided based on vertical and horizontal proportion maps, which are used to create proportion volumes for each facies (**Figure 4**). The facies are then interpolated through the volumes and check that the interpolation matches with the current understanding of each sub-region.
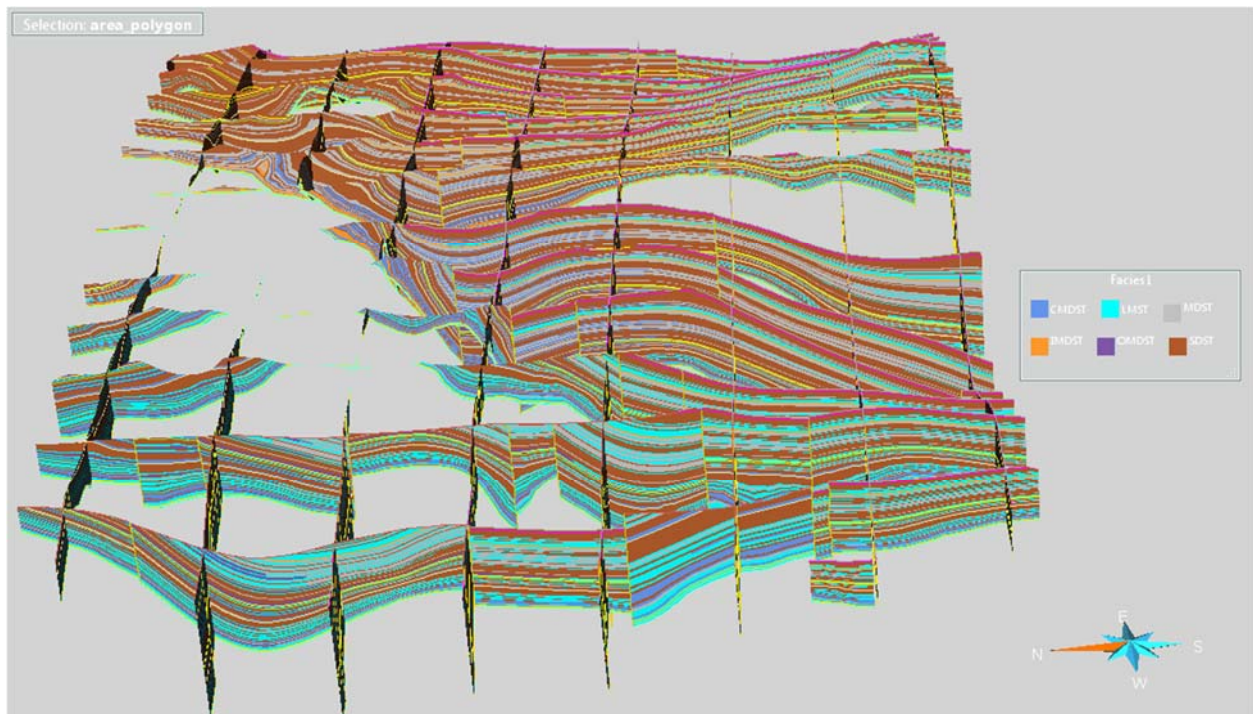
Figure 4 Interpolated facies showing predominance of limestone and carbonaceous mudstones and sandstone facies.

3.2   DATABASE OF SAMPLE ANALYSES

The BGS introduced a digital database system for sample analysis data in 2013. Prior to this, data was held as hard copy, with a high-level digital index. Once submitted, data remains confidential for 2 years following the date of sampling, with interpretative reports confidential for 5 years. Data originating from sampling post-dating 2014 is therefore released and available to third parties, with data basing activities currently ongoing. Work continues to identify analytical data submitted prior to 2013.

3.3   FUTURE OPTIONS

Progress analysis and modelling of age-equivalent units across Bowland-Hodder subcrop;

Progress database of unpublished biostratigraphical and analytical (Rock Eval; X-ray diffraction) data held by BGS of Bowland-Hodder unit;

Develop palaeofacies maps;

Develop predictive models.

4 Work Package 3: Development of chemical stratigraphies through prospective parts of the stratigraphic column

4.1 ROCK-EVAL(6) GEOCHEMICAL EVALUATION OF OUTCROP SAMPLES

Sites of outcrop were visited and sampled from the Clitheroe (Lancashire) and Edale (Derbyshire) areas. Twenty-six outcrop samples were evaluated for unconventional hydrocarbon potential using Rock-Eval6 analyses (figures 5, 6, and Appendix 1). Organic carbon content ranged from 0.73 to 4.66 % with present day HI of 20 to 210 mg/g TOC. All the samples yielded original hydrogen index (HIo) values > 250, a value broadly indicative of shale gas potential. However, the Tmax value (a proxy for thermal maturity) suggested nearly all the outcrop samples were too immature to have generated appreciable amounts of dry gas (Edale Basin outcrop samples mean Tmax 447°C and Craven Basin outcrop samples mean Tmax 441 °C). The shale-oil potential of each borehole was also considered using the oil saturation index, none of the outcrop passed the >100 mg/g TOC benchmark, suggesting that these are not prospective for shale-oil. This study shows that weathered samples (subject to post burial alteration) can be identified on the basis of elevated oxygen indices which in turn suggests that the majority of outcrop samples are relatively unaltered (in terms of hydrocarbon geochemistry), and therefore suitable for inclusion in the dataset describing the organic character of shale samples within the project area.
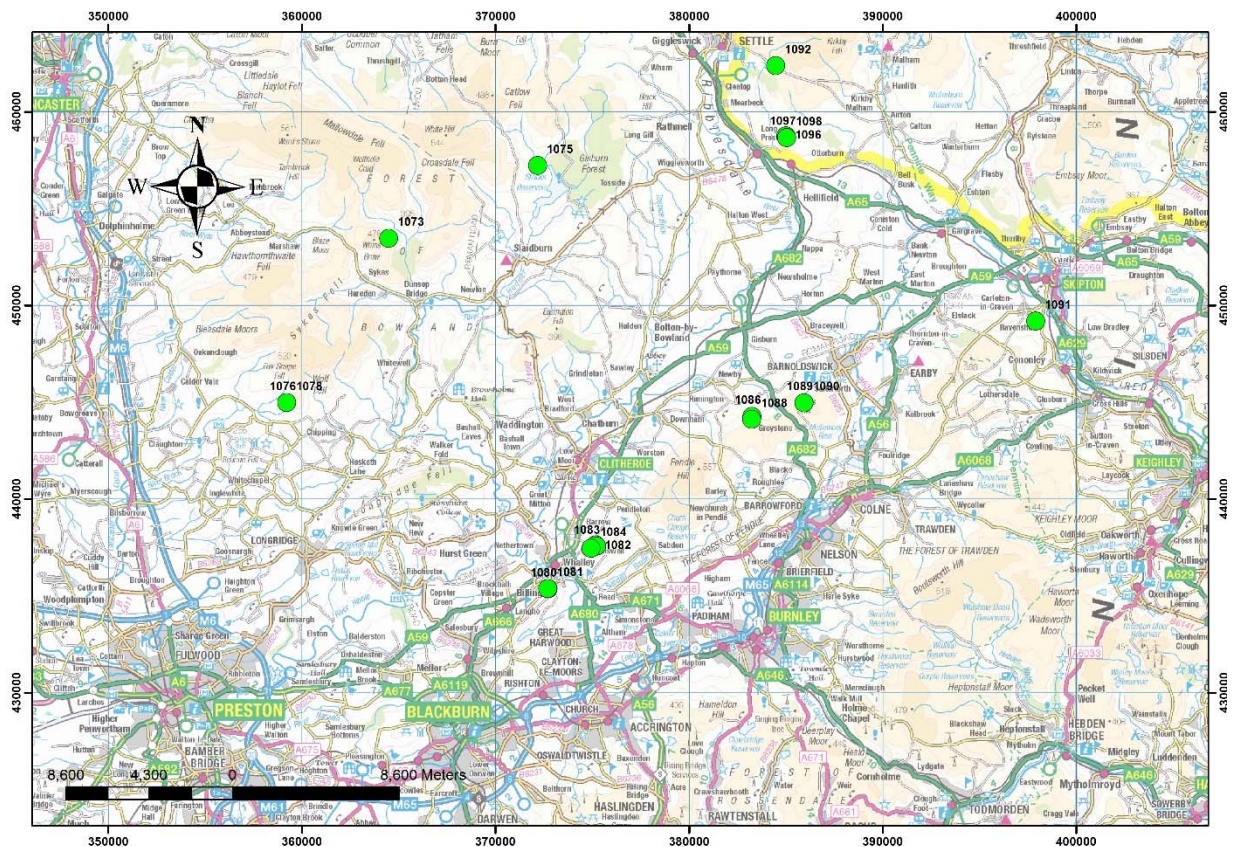
Figure 5 Sites of outcrop samples taken for analysis (Clitheroe area)
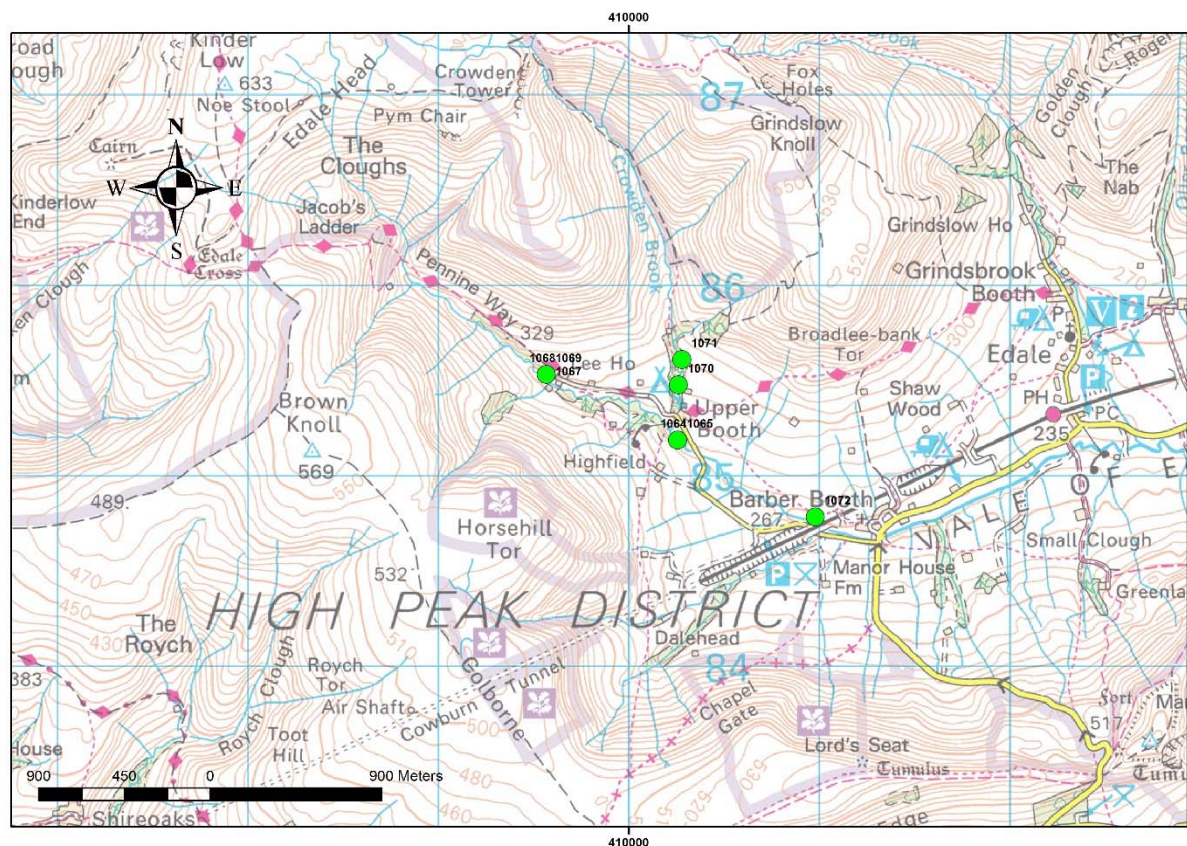
Figure 6 Sites of outcrop samples taken for analysis (Edale area)

4.1.1   Outcrop selection and analytical method

Twenty six outcrop samples comprised of calcareous mudstone, carbonaceous mudstones (Shale) and ferruginous mudstones of varying age (Table 2) were taken from outcrop and analysed using the BGS Rock-Eval instrument.

Table 2 Substage of samples analysed for Rock Eval and XRD

Regional Substage	Number of samples analysed
Kinderscoutian	3
Chokeirian	2
Arnsbergian	2
Pendleian	11
Brigantian	8

Samples were analysed using a Rock-Eval(6) analyser configured in standard mode (pyrolysis and oxidation as a serial process). Powdered rock samples (60 mg /dry wt) were heated isothermally at 300ºC for 3 min and then heated from 300 to 650ºC at 25ºC/min in an inert atmosphere of N_2 and the residual carbon was then oxidised from 300ºC to 850ºC at 20ºC/min (hold 5 min). Hydrocarbons released during the two stage pyrolysis were measured using a flame ionization detector and CO and CO_2 measured using an IR cell.

The performance of the instrument was checked every 10 samples against the accepted values of the Institut Français du Pétrole (IFP) standard (IFP 160 000, S/N15-081840). In addition the main parameters derived from the data include Production Index (PI), Hydrogen Index (HI) and Oxygen

Index (OI). PI is the sum of the S1 and S2 hydrocarbons. HI is calculated from the ratio of S2 mg HC per gram of organic carbon and values above 350 are said to be good source rocks (for conventional hydrocarbons, Tissot & Welte 1978, fig. V.1.11). OI is the ratio of mg carbon dioxide per g organic carbon. HI and OI are plotted to be comparable with the van Krevelen diagram, showing the branching of the different kerogen types I (lacustrine, algal, oil prone), II (marine, oil prone), III (terrestrial, gas prone) and IV (oxidised or inertinite).

4.1.2   Total organic carbon (TOC)
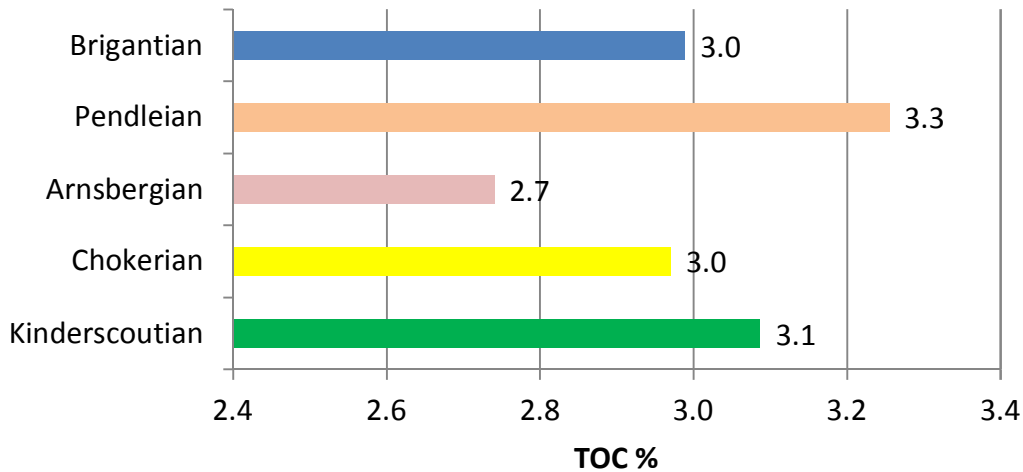
Figure 7. Mean Total Organic Carbon (% wt/wt) from Carboniferous shales classified on the basis of Substage.
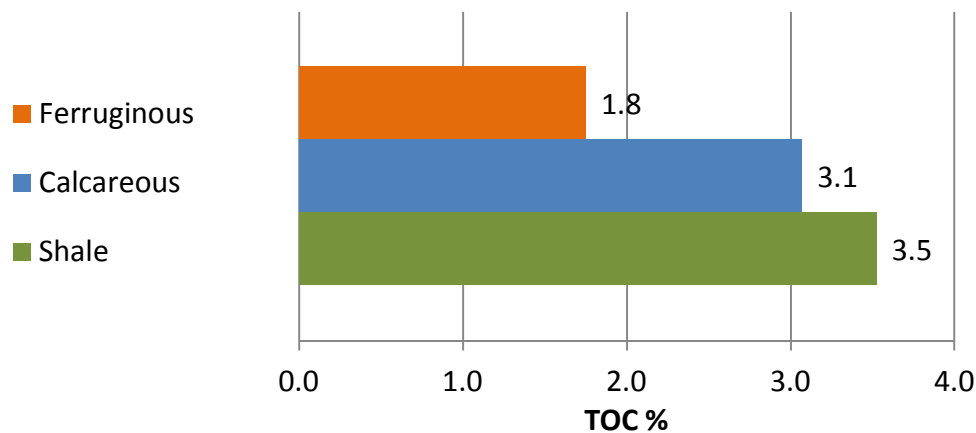
Figure 8. Mean Total Organic Carbon (% wt/wt) from Carboniferous shales classified on the basis of lithology.
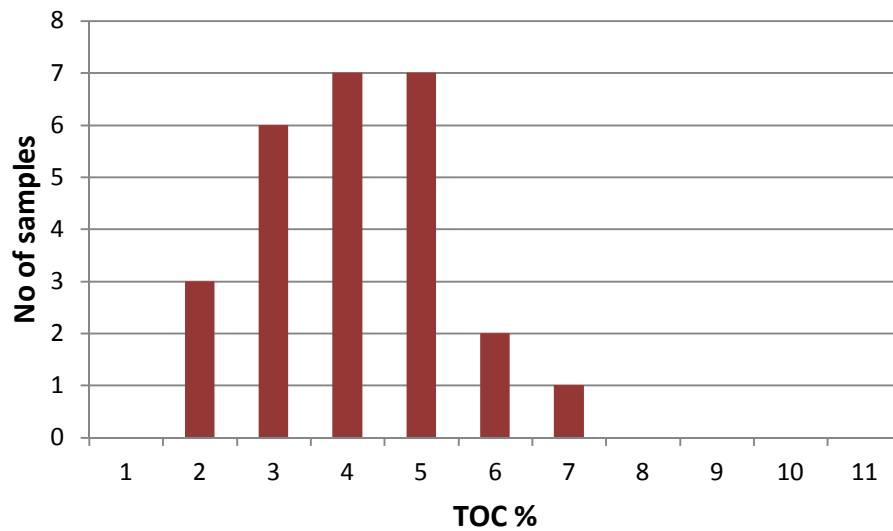
Figure 9. TOC frequency distribution of Carboniferous shales from selected outcrops representing three lithologies.
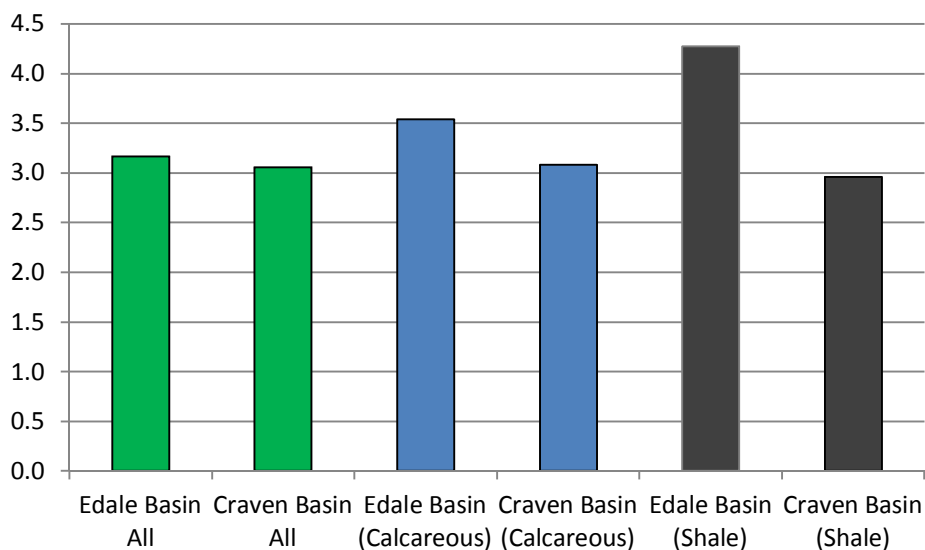
Figure 10. Comparison of mean TOC % values from Edale and Craven Basins.

From a stratigraphic standpoint, outcrop samples from the Pendleian and Kinderscoutian substages gave the highest mean % TOC of 3.3 and 3.0 respectively (Figure 7). Comparison of mean TOC from all five substages showed similar values in the range of 3.3 to 2.7 %. Whereas mean TOC content of weathered (ferruginous) as compared to carbonaceous shales and calcareous sediments were markedly different 1.8 to 3.1 and 3.5 % (Figure 8). Inspection of the frequency of TOC distribution showed that many of the samples from outcrop had good TOC (>2%) (Figure 9). Comparison of TOC % from lithologicaly equivalent facies from Edale and Craven Basins showed that both have similar average TOC contents ~3 (Figure 10). However, rather surprisingly TOC content were higher in both calcareous and carbonaceous shales outcrop samples from the Edale Basin than the Craven Basin.

11

4.1.3   Organic Matter Type and Hydrocarbon Potential
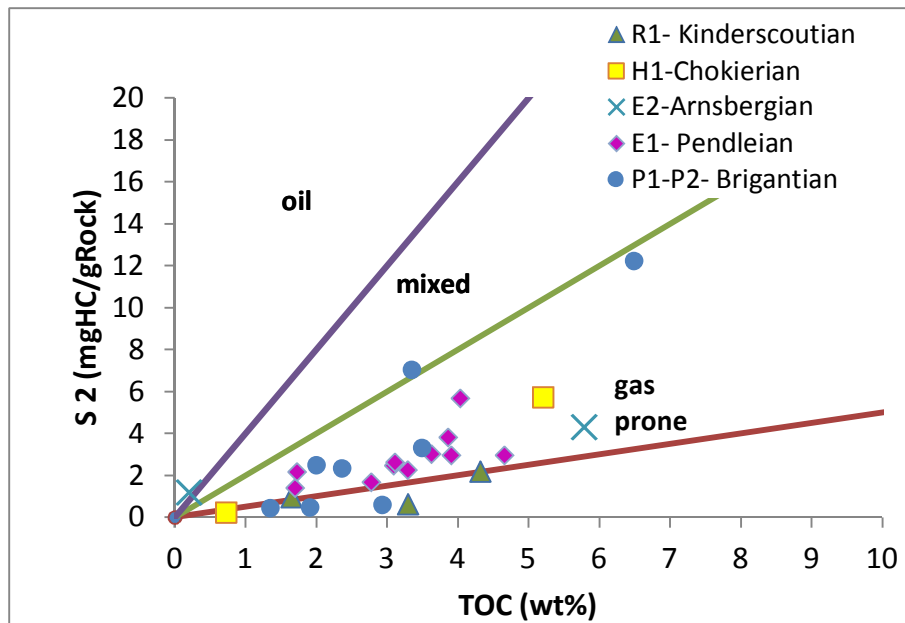
Figure 11. **Bi-Plot showing TOC against bound hydrocarbons (S2). Outcrop groupings based on geological age (substage).**
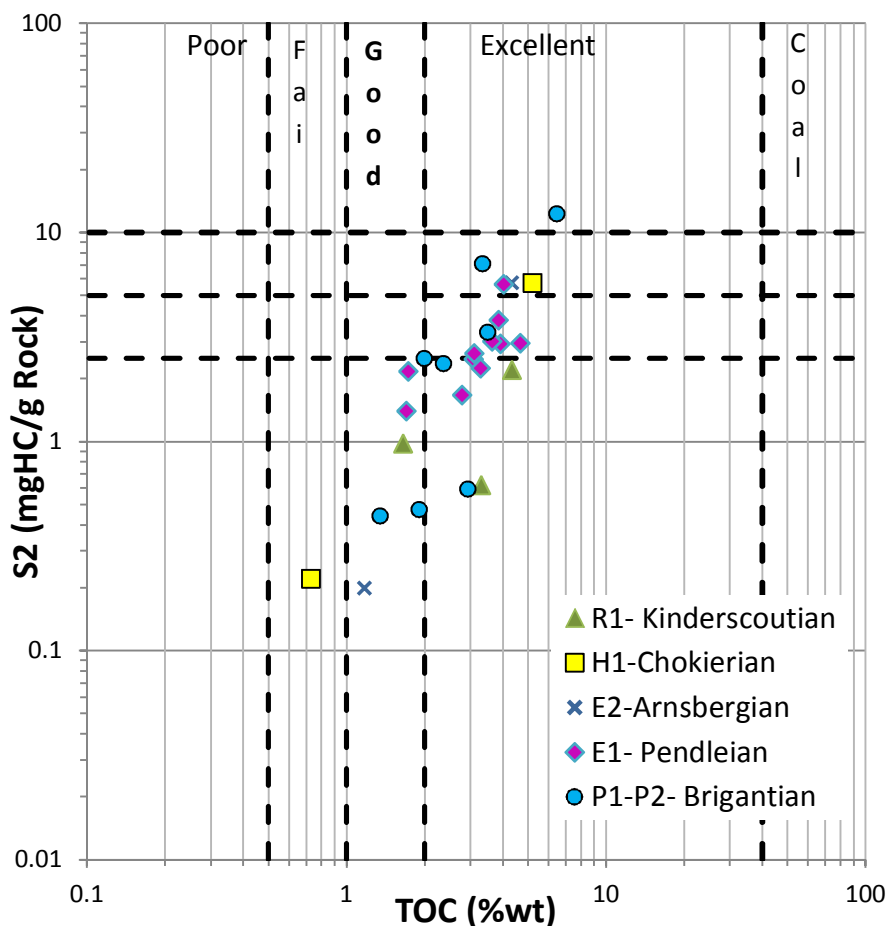
Figure 12. **Generational potential as evaluated from a traditional hydrocarbon standpoint.**

In conventional source rock evaluations the type of hydrocarbon generated maybe be estimated based on relationships between bound hydrocarbons (S2) and TOC (Slowakiewicz et al., 2015). Inspection of Figures 11 and 12 suggests that the majority of outcrop samples are gas prone with the exception of two samples from Brigantian-aged strata. From a conventional oil play standpoint

the twenty six outcrop samples span fair to excellent classification, although the majority only fall within the fair (y axis) criteria (Figure 12). However, although measurement and interpretation of generative potential (S2) and TOC are useful, these values can be influenced by increasing maturity and become less reliable as values approach the origin.

It is generally accepted that a high initial (original) hydrogen index and low oxygen index are universally desirable whether conventional or unconventional systems. In conventional petroleum settings high present day HI values >300 are considered key whereas in unconventional accumulations HI present day values of <60 can generate successful shale gas plays (e.g. Barrnett Shale, Fort Worth Basin) due to the cracking of the kerogen directly to gas and also of kerogen to expelled oil to gas which in turn is observed in Rock-Eval analyses as a decrease in HI with increasing maturity. Consequently although the present day HI values for the outcrop samples were fairly low ranging from 17 to 210 mg/g TOC they cannot be entirely excluded as potential shale gas resources. However, the low HI values are problematic in that they confound a definitive organic matter type classification, because they plot toward the origin where Types I, II and III kerogens converge. On balance, the majority of the outcrop samples probably contain a mix of II/III organic matter. In contrast three samples have OI values >40 (44 to 208) which suggests that these had undergone extensive oxidative alteration and are classified as Type IV kerogens (Figure 13). Unfortunately, it is not possible to ascertain whether the oxidative alteration occurred before or during burial or alternatively occurred as a consequence of modern day weathering of the outcrop.

Prospective shale gas plays in general have kerogen quality as determined from the original hydrogen index (HIo) in general these require HIo value of > 250. The original Hydrogen index were calculated following a method similar to that previously published (Jarvie, 2012) The Edale Mudstones gave HIo of 451 and Craven Basin HIo of 472 mg/g TOC which falls above the accepted benchmark (Jarvie, 2012).
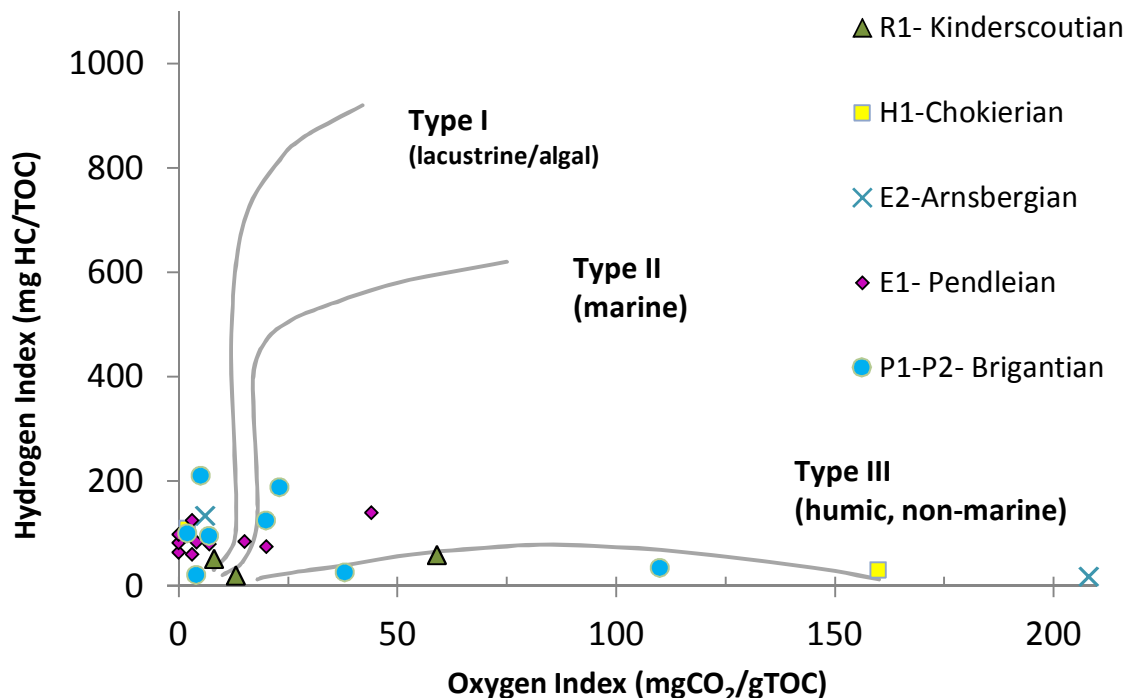
Figure 13. **Modified van Krevelen bi-plot showing broad organic groupings, with increasing maturation all organic matter trends toward the origin.**
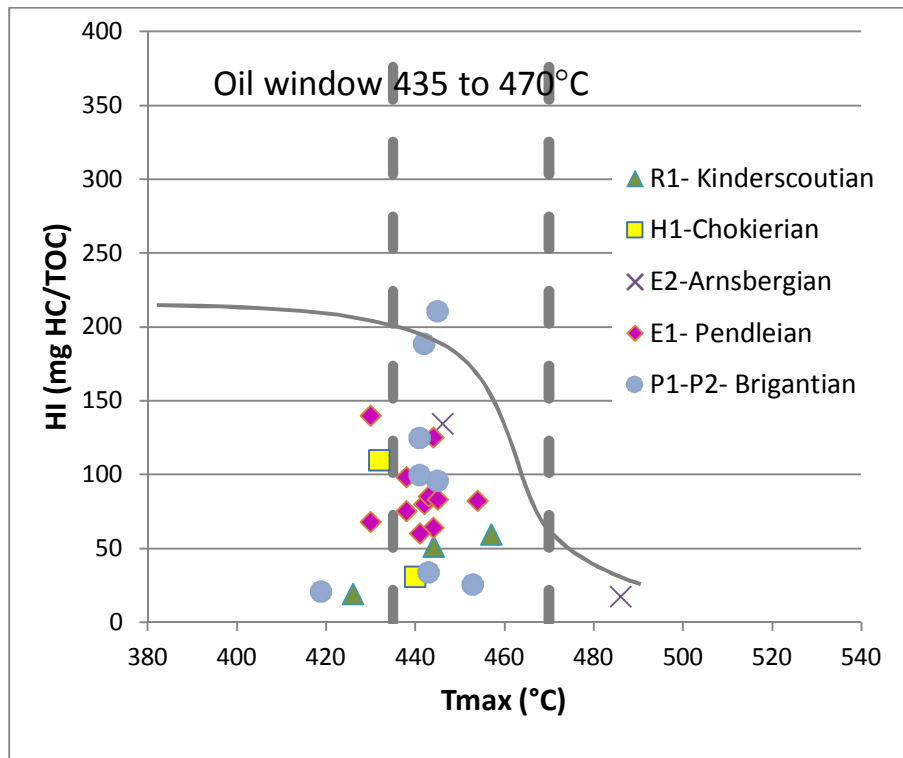
Figure 14. Maturity bi-plot (Tmax) and organic matter richness (HI). Groupings based on age (substage).

4.1.4 Maturity

Prospective shale-gas plays in general have thermal maturities of about >470°C Tmax this is equivalent to a thermal maturity as measured using optical methods of about VRo 1.4 %. It should be borne in mind that gas begins to be generated about mid-way in the oil window and extends beyond Tmax 550°C or VRo 2 %. In general Tmax values below 435°C are considered immature, values between 435 and 470 yield oil those beyond 470°C generate appreciable amounts of gas either as wet gas or as maturation increases dry gas. In this study the Edale and Craven Basin outcrop samples show a range of Tmax values across the oil window and would be considered moderately prospective for gas based on Rock-Eval maturity (figures 13, 14). Five samples were too immature to have generated oil or gas, twenty were within the early to mid oil window and only one sample is mature enough to be considered a true shale gas prospect , as it lies on the boundary between the end of the oil window (mean Tmax 486°C), close to peak wet gas generation.

4.1.5 Shale-oil potential

The hydrocarbon potential of shale-oil systems can be assessed using the oil saturation index (OSI: $S1 \times 100 / TOC$); potential resources are identified using empirical OSI values >100 mg/g TOC (Lopatin et al., 2003; Slowakiewicz et al., 2015). The premise here is that organic matter sorbs oil generated at values <100 mg /g TOC and that the sorption threshold is exceeded at OSI >100 (the "oil cross-over"). OSI values for the successions analysed from the eight borehole ranged from 7 to 38 mg/g TOC (n=127) (Table 3), which falls well below the 100 mg cut-off and indicates that the Upper Carboniferous mudrock analysed herein do not contain enough oil (free-sorbed oil) to be considered a viable shale-oil resource

Table 3. Assessment of boreholes shale-oil potential using oil saturation index (OSI) criteria

Basin/Sub Basin	Borehole	Arithmetic Mean Oil Saturation Index (OSI mg/g TOC)	Range of Oil Saturation Index (OSI mg/g TOC)
Harrogate Basin			
	Marsden	7	4-11
	Crimple Beck	15	5-32
	Butterhaw	13	12-15
Craven Basin			
	Withgill Farm	29	18-38
	CowArk 7	18	11-23
Cleveland Basin			
	Malton 4	8	7-11
Widmerepool Gulf			
	Lees Farm	23	10-23
	Wetton	20	10-32

*a Value >100 OSI is the minimum requirement for a potential shale-oil resource.

4.1.6 Lithological description compared to geochemical measurement

The twenty six outcrop samples were identified in the field and classified based on visual appearance as limestone, calcareous mudstone or dolomitic sandstone. A comparison was made between these field descriptions to the rarely utilised % mineral C parameter in order to assess the utility; for example, pure calcite yields a Min C of 12.59 % and pure Dolomite gives Min C of 13.16 %. In this current study comparison of the mineral C % showed that samples assigned calcareous identification had a MinC value of 0.20 to 9.99 with a mean of 3.52 % whereas the mudstones ranged from 0.12 to 5.71 with a mean of 0.93 % which suggests the Rock-Eval min C can identify calcareous samples.

4.1.7 Conclusions

This work demonstrates that if carefully selected, material at outcrop can be used to characterise the hydrocarbon content and contribute to the understanding of the shale hydrocarbon resource in the Edale and Craven Basins. Material which has undergone extensive modern day surface weathering can be identified due to elevated OI values which suggests oxidative alteration of the organic matter.

4.2 FUTURE OPTIONS

Further work investigating the organic geochemistry of the Bowland Shale will include the detailed sampling of identified marine band horizons from boreholes not previously used in this study. The available borehole material includes boreholes drilled for mineral exploration and that recently drilled and released in the north-western part of the project area, where there is a greater degree of stratigraphic control.

5 Work Package 4: Hydromechanical behaviour of shales

5.1 REVIEW OF AIM OF WP4

The primary aim of this Work Package is to increase our understanding of hydraulic fracturing in Bowland shale. The success of any unconventional play will not only depend on the overall quantity of gas or oil present, but on the ability to recover the gas; central to the recoverability is the interaction of pre-existing discontinuities (fractures, faults, joints etc) in the shale with fractures formed by hydraulic stimulation of the formation. While our understanding of hydraulic fracturing processes is adequate, there are still a number of key unknowns as to the geometry and extent of fractures created.

Work Package 4 has been divided into four sub-tasks:

- WP4.1 examines the geomechanical properties of Bowland shale
- WP4.2 investigates the transport properties (permeability, storage etc) of Bowland shale
- WP4.3 aims to extend our knowledge of hydraulic fracture formation
- WP4.4 aims to answer key societal questions related to hydraulic stimulation and associated risks

5.2 WP4.1 GEOMECHANICAL PROPERTIES

Samples were taken from two boreholes, Crimple Beck and Cow Ark 7, for geotechnical index testing in the laboratory; specifically Point Load Strength Index (Figure 16) plus a limited number of Uniaxial Compressive Strength (UCS) tests. In addition, a limited number of trial tests using the FRACKiT apparatus.

5.2.1 WP4.1.1 Variation of strength of Bowland shale

This task will measure standard strength parameters for a complete sequence of Bowland shale from existing BGS core material. A variety of standard strength tests will be conducted.

5.2.1.1 SAMPLE PREPARATION

Samples from both boreholes were in a dried out state. Samples from the Crimple Beck borehole were 78 mm diameter and split across the core into 'disks', presumably due to both drilling disturbance and desiccation, and only fragments were available for trimming for the Point Load Strength Index test using the procedure for 'irregular lumps' (Ulusay & Hudson, 2007). Parts of the core had been slabbed and were also prepared as 'irregular lumps'. Samples from Cow Ark 7 were cores of 26.5 mm diameter (unslabbed) and were therefore available for trimming for the Point Load Strength Index test using the procedure for 'cylinders' (Ulusay & Hudson, 2007).

The approximate ranges of applicability of various rock strength tests are shown in Figure 15.
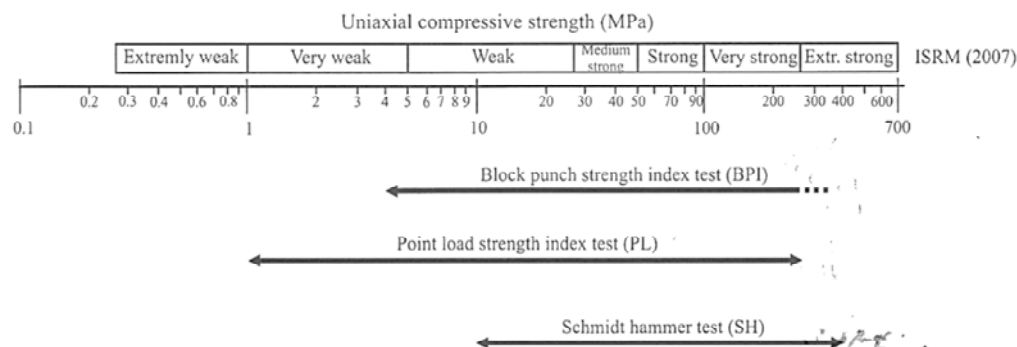
Figure 15 Table showing applicability of selected strength index tests (adapted from Ulusay & Hudson, 2007)

5.2.1.2 POINT LOAD STRENGTH INDEX

The Point Load Strength Index test (Ulusay & Hudson, 2007) is a simple index test, the results of which can be used to correlate with rock strength. The Point Load Strength Index (PLSI) tests were carried out using an ELE International instrument (Figure 16). This features a digital stress readout with maximum hold readout function and a hand-operated jack capable of applying a force, *P* of up to 50 kN to a pair of opposing cone-shaped hardened steel platens. The distance between these platens prior to testing, with the test specimen in place between the cones, is taken as dimension *D* (mm) and read from a steel scale fixed to the apparatus. The apparatus is contained in a purpose-built Perspex cabinet to prevent rock fragments flying out during the test.

Figure 16 Point Load Strength Index apparatus (ELE International)

There are two versions of the test: the first utilises a cylindrical core sample, either taken directly from borehole core or machined. This test is referred to as 'CYLINDER'. The second utilises an irregularly-shaped lump of rock. This is referred to as 'IRREGULAR'. In the former case the two dimensions, half-length and diameter are measured using a ruler and recorded, while for the latter the two cross-sectional (average) dimensions, width and depth, that is in the same plane as the applied stress, are measured and recorded. The cylinder test itself has two versions: one where the force is applied diametrally and the other where it is applied axially. The irregular test has the option of applying the force either parallel or perpendicular to the bedding or foliation. In fact, these options can also be applied to the diametral 'cylinder' test by rotating the specimen between the cones should the bedding/foliation not be perpendicular to the core.

5.2.1.3 CYLINDER TEST

For tests on cylindrical specimens, the point load strength, $I_{S(50)}$, and the strength anisotropy index, $I_{a(50)}$, were calculated using the following formulae:

$$I_{a(50)} = \frac{I_{S(50)} \; perpendicular \; to \; lamination}{I_{S(50)} \; parallel \; to \; lamination}$$

$$I_{S(50)} = FI_S \qquad F = \left(\frac{D_e}{50}\right)^{0.45} \qquad I_S = \frac{P}{D_e^2}$$

$$D_e^2 = D^2 \text{ (for diametral tests)} \qquad D_e^2 = \frac{4A}{\pi} \text{ (for axial tests)}$$

Where $I_{s(50)}$ is the corrected Point Load Strength Index (normalised to $D_e = 50$ mm²), $I_{a(50)}$ is the strength anisotropy index, I_s is the uncorrected Point Load Strength Index, P is the maximum load measured prior to failure (N), F is the size correction factor, D_e is the equivalent core diameter (mm), D is the core diameter (mm), H is the core thickness (axial tests) (mm), and A is the minimum cross sectional area of a plane through the platen contact points (mm²).

The restrictions on permitted specimen dimensions are shown in Figure 17. The cylinder half-length (L) in the diametral test must be greater than half the diameter. This is to ensure that the tensile failure mode does not feature a significant longitudinal component. In the axial test the core thickness (between the platens) must exceed a third of the diameter but be less than the diameter.
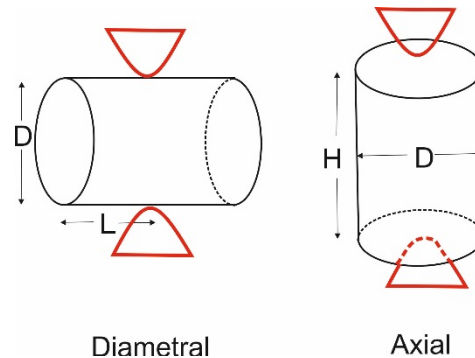
Diametral   Axial
Figure 17 Dimensions of point load strength index specimens (cylindrical specimen)

5.2.1.4 IRREGULAR LUMP TEST

The irregular test is carried out on irregular-shaped lumps of rock or pieces of broken core which do not satisfy the conditions for a cylinder test (Figure 18).
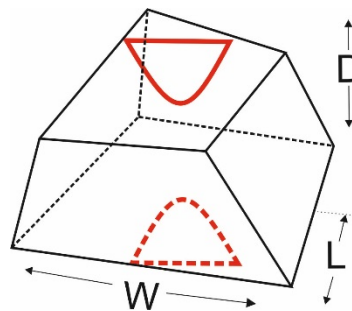
Figure 18 Dimensions of irregular specimen

The PLSI test procedures used matched those recommended (Ulusay & Hudson, 2007) with the exception of the '10 specimens per test' criterion. It was not possible to comply with this due to the limited size of samples available. As a result, statistical elimination of the highest and lowest values was not possible, except in a very few cases. However, the failure mode criteria were adhered to and 'incorrect' failure modes were not included in the results. A significant proportion of tests exhibited elements of pre-failure deformation. These results were retained provided that they didn't contravene the failure mode criterion described previously.

The values of $I_{s(50)}$ from the perpendicular PLSI tests for Crimple Beck (Figure 19) range from 1.0 to 9.9 and for the parallel PLSI tests from 0.1 to 9.1; the averages were 3.3 and 1.8, respectively.

The values of $I_{s(50)}$ from the axial PLSI tests for Cow Ark 7 (Figure 20) range from 1.1 to 6.4 and for the diametral PLSI tests from 0.2 to 12.4; the averages were 3.1 and 2.8, respectively.
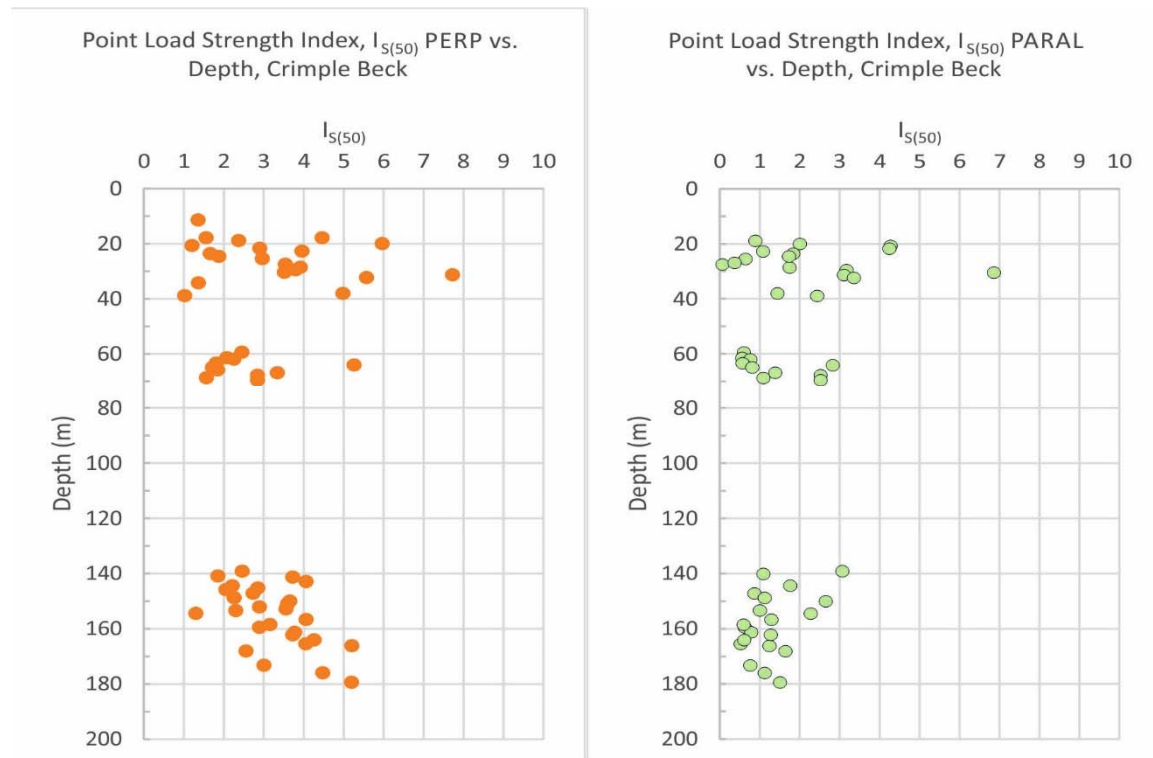
Figure 19 Plot of Point Load Strength Index, $I_{S(50)}$ vs. Depth for Crimple Beck (left: perpendicular to bedding, right: parallel to bedding).

The strength anisotropy results are shown with depth for Crimple Beck in Figure 21. Values of I_a range from 0.3 to 7.6 for Crimple Beck and the average is 2.6. The strength anisotropy results for Cow Ark 7 are shown in Figure 21. Values of I_a range from 0.3 to 5.2 and the average is 1.7.

The scatter of data is considerable, but not unexpected for this type of index test. A significant number of data points, from both boreholes, show $I_a < 1.0$ indicating that values parallel to bedding here exceeded those perpendicular to bedding. In some cases this was due to the presence of well-cemented crystalline bedding deposits in the failure zone imparting greater 'parallel' strength than normal for the host rock. Conversely, the higher values of I_a ($I_a > 2$) indicate greater fissility and hence the presence of weak, uncemented bedding planes in the failure zone. A very small number of test specimens also featured slickensided surfaces.

19
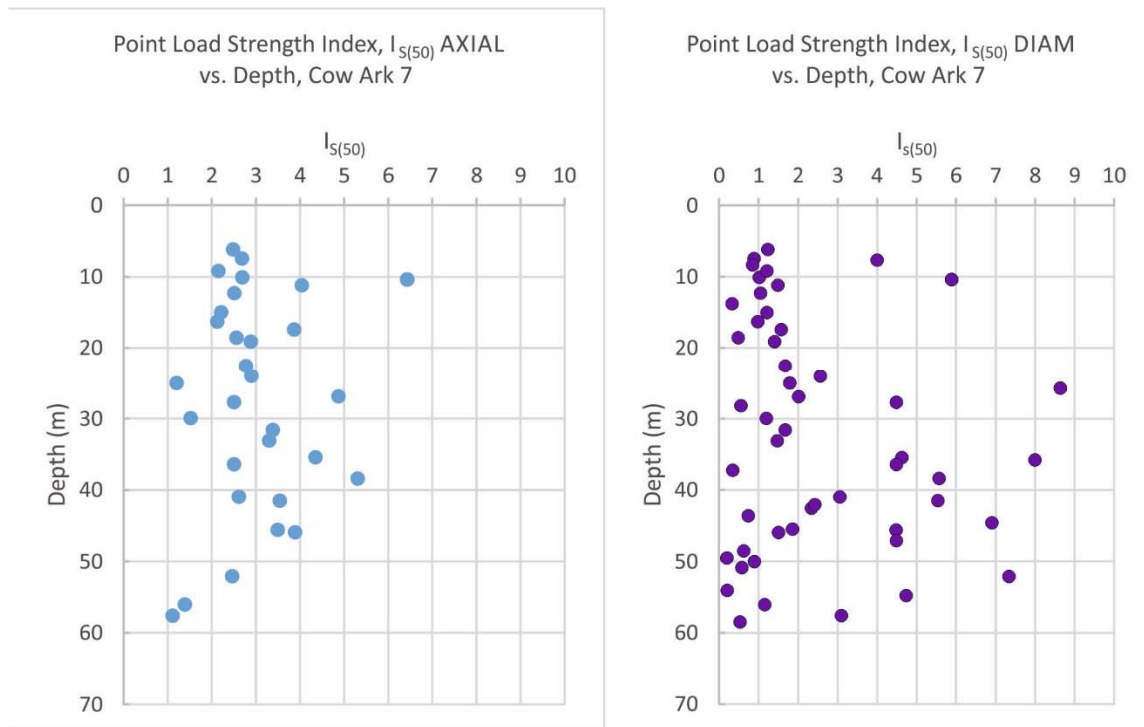
Figure 20 Plot of Point Load Strength Index, $I_{S(50)}$ vs. Depth for Cow Ark 7 (left: axial to core, right: diametral to core)
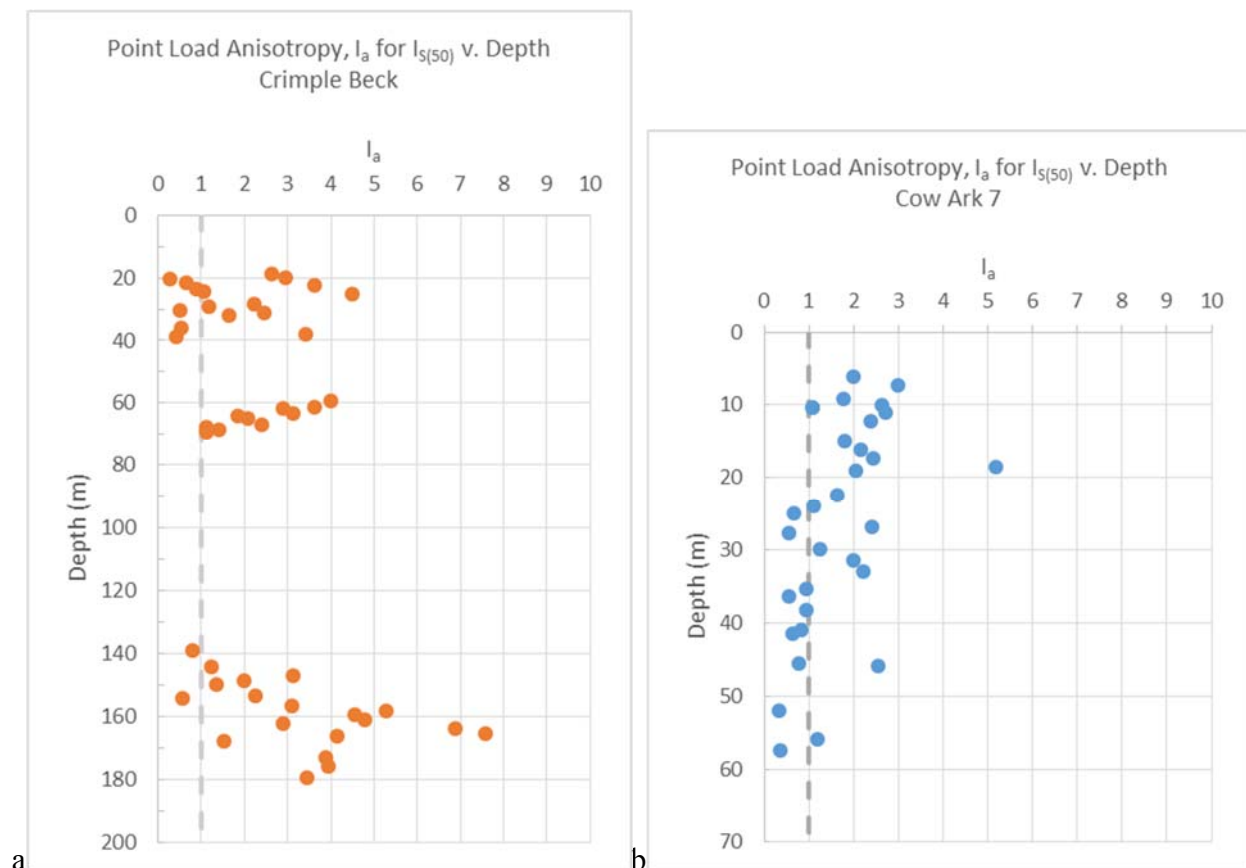
Figure 21 Plot of Point Load Anisotropy, I_a vs. Depth. a) Crimple Beck (Note: $I_a = I_{s(50)} PERP / I_{s(50)} PARAL$); b) Cow Ark 7 (Note: $I_a = I_{s(50)} AXIAL / I_{s(50)} DIAM$)

Trends of I_a with depth are poorly defined. For example, there is the suggestion of a trend of decreasing I_a with depth for Cow Ark 7 and localised trends of decreasing I_a between 60 m and 70 m depth and increasing I_a between 139 m and 180 m depth for Crimple Beck; the shallower of

these for Crimple Beck probably being the clearest. Unfortunately, there is not a continuous record with depth for Crimple Beck.
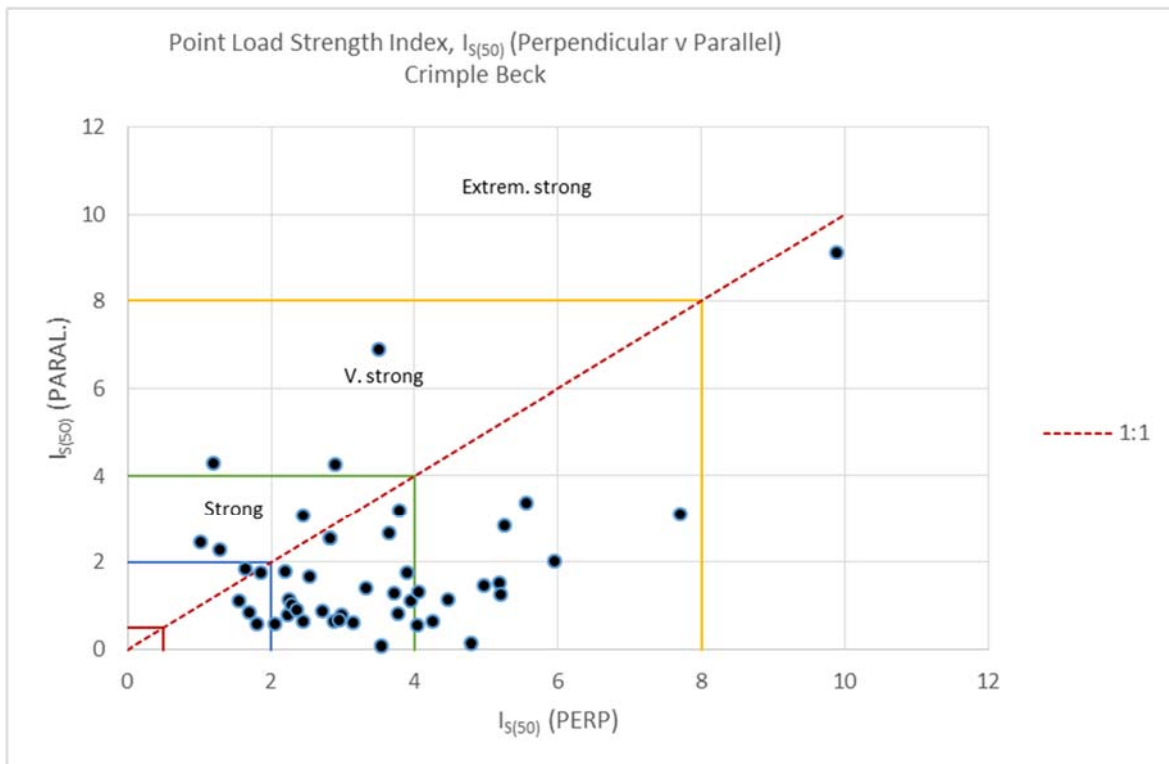
Figure 22 Plot of PLSI (perpendicular to bedding) vs. PLSI (parallel to bedding) for Crimple Beck
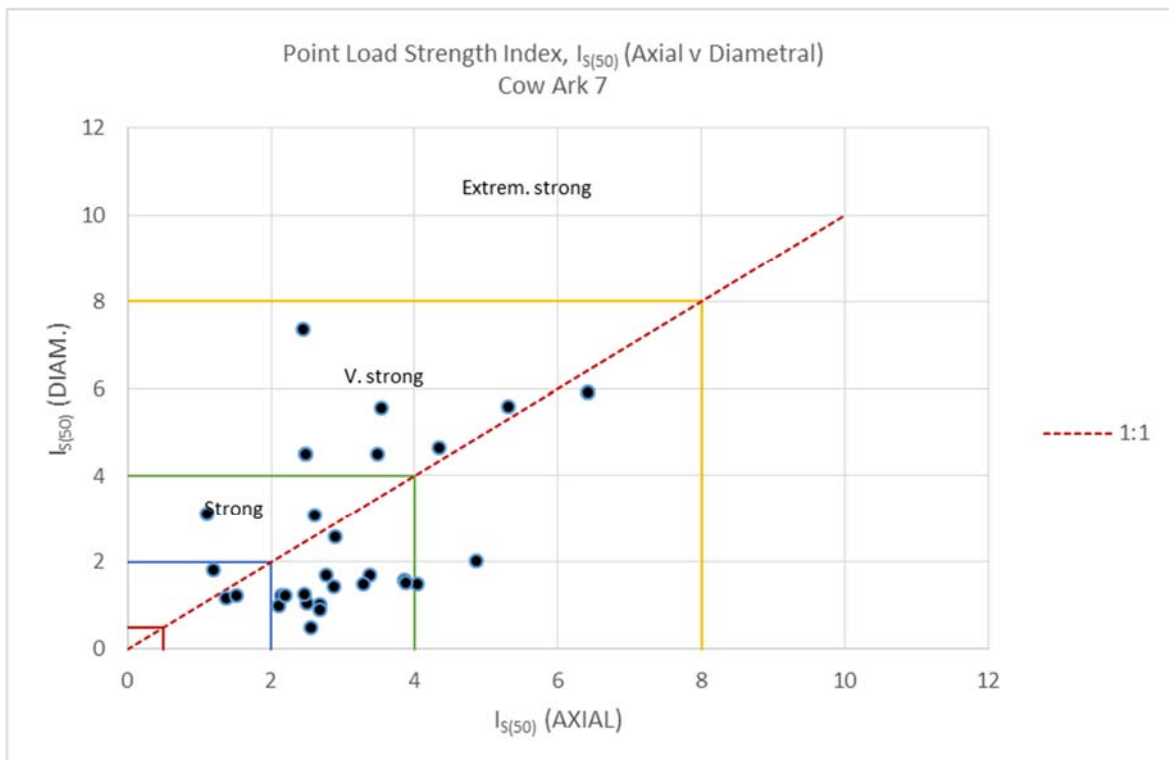
Figure 23 Plot of PLSI (axial) vs. PLSI (diametral) for Cow Ark 7

It should be noted that whilst the cylindrical specimens tested from Cow Ark 7 could be rotated between the cone platens to favour, in most cases, a failure surface parallel with the bedding, it

was not always possible to achieve this for the specimens from Crimple Beck as this depended on the irregular facets of the 'lump' specimen in relation to the bedding. In practice most, but not all, tests resulted in failure along bedding

The Point Load Strength Index test results can be converted to 'equivalent UCS' using the following well documented relationship:

$$Eq\ UCS = I_{s(50)} \times 24.0$$

This conversion gave a Eq UCS range of 25 to 237 MPa with an average of 79 MPa for Crimple Beck (perpendicular to bedding) and 2 to 218 MPa with an average of 43 MPa for Crimple Beck (parallel to bedding). It gave a range of 5 to 297 MPa with an average of 66 MPa for Cow Ark 7 (axial) and 5 to 297 MPa with an average of 66 MPa for Cow Ark 7 (diametral). These results place the Bowland Shale samples in the classification ranges 'very weak' to 'very strong' with the averages 'medium strong' to 'strong' (figures 22, 23).

However, other conversion factors specifically for mudstone and siltstone (between ×12 and ×15) have been suggested elsewhere (Kahraman, 2001; Singh et al, 2012). Based on the lower of these values (×12) the UCS is now halved; giving the range of UCS from 12.5 to 118.5 MPa with an average of 39.4 MPa for Crimple Beck (perpendicular to bedding) and 1.0 to 109.0 MPa with an average of 21.6 MPa for Crimple Beck (parallel to bedding). It gave a range of 13.5 to 77.0 MPa with an average of 37.2 MPa for Cow Ark 7 (axial) and 2.5 to 148.5 MPa with an average of 33.2 MPa for Cow Ark 7 (diametral).

Considering a conversion of PLSI results to equivalent indirect tensile strength (Eq. ITS), as for example obtained from a Brazilian Disc test, a conversion factor of ×0.8 was used as recommended in Ulusay & Hudson (2007). Eq. ITS results range from 0.83 to 7.90 MPa with an average of 2.63 MPa for Crimple Beck (perpendicular to bedding) and 0.07 to 7.27 MPa with an average of 1.44 MPa for Crimple Beck (parallel to bedding). It gave a range of 0.90 to 5.14 MPa with an average of 2.48 MPa for Cow Ark 7 (axial) and 0.17 to 9.90 MPa with an average of 2.21 MPa for Cow Ark 7 (diametral).

The PLSI and derived results described above are summarised in Table 4 and Table 5.

Borehole		$I_{s(50)}$ PERP.	$I_{s(50)}$ PARAL.	Ia	Eq. UCS *PERP.* X24	Eq. UCS *PARAL.* X24	Eq. UCS *PERP.* X12	Eq. UCS *PARAL.* X12	Eq. ITS *PERP.* X0.8	Eq. ITS *PARAL.* X0.8
					(MPa)	(MPa)	(MPa)	(MPa)	(MPa)	(MPa)
Crimple Beck	Min	1.0	0.1	0.3	25.0	2.0	12.5	1.0	0.83	0.07
	Max	9.9	9.1	7.6	237.0	218.0	118.5	109.0	7.90	7.27
	Average	3.3	1.8	2.6	79.0	43.0	39.4	21.6	2.63	1.44

Table 4 Summary of Point Load Strength Index test results and derived results (Crimple Beck) (UCS: Uniaxial Compressive Strength)

Borehole		$I_{s(50)}$ AXIAL	$I_{s(50)}$ DIAM.	Ia	Eq. UCS *AXIAL* X24	Eq. UCS *DIAM.* X24	Eq. UCS *AXIAL* X12	Eq. UCS *DIAM.* X12	Eq. ITS *AXIAL* X0.8	Eq. ITS *DIAM.* X0.8
					(MPa)	(MPa)	(MPa)	(MPa)	(MPa)	(MPa)
Cow Ark 7	Min	1.1	0.2	0.3	27.0	5.0	13.5	2.5	0.90	0.17
	Max	6.4	12.4	5.2	154.0	297.0	77.0	148.5	5.14	9.90
	Average	3.1	2.8	1.7	74.0	66.0	37.2	33.2	2.48	2.21

Table 5 Summary of Point Load Strength Index test results and derived results (Cow Ark 7) (UCS: Uniaxial Compressive Strength)

5.2.1.5 UNIAXIAL COMPRESSIVE STRENGTH (UCS) TESTS

A small number of Uniaxial Compressive Strength (UCS) test specimens were prepared from Cow Ark 7 core. The core has a diameter of 26.5 mm and therefore the UCS test specimens prepared from it could not be considered as compliant with standard procedures, due to being undersize (Ulusay & Hudson, 2007). However, the length to diameter ratio was maintained close to 2:1 in all cases. The UCS tests have yet to be conducted.

5.2.2   WP4.1.2 Development of FRACKiT

The new FRACKiT test is designed to allow a simple (indirect) tensile strength test to be carried out on core samples of rock types for which machining is either unavailable or impossible. The test method causes a compressive force to be applied within a drilled hole which nevertheless results in a particular form of tensile failure whereby a fracture develops instantaneously across a diametral plane splitting the core in two. No confining stresses are involved and the test specimen is not machined externally. The inflation of a bore can be seen to be analogous to the loading that occurs during hydraulic fracturing.

The new FRACKiT apparatus, having being originally designed at BGS for testing 'extremely weak' rocks and referred to as a 'mini-pressuremeter' (Hobbs et al., 1997), was modified to extend the testing range to 'very weak' and 'weak' rocks, for example some types of shale and mudstone. The principle of the apparatus is that a small probe, having a nitrile rubber bladder, inserted into a 10 mm hole drilled diametrally in the core, is inflated by filling with de-aired water using a syringe pump. The pressure and volume of fluid applied is ramped up and measured with time to the point where tensile failure of the core occurs. The original calculations to determine indirect tensile strength are based on those for a full-scale borehole pressuremeter (Mair & Wood, 1987; Clarke, 1995), the principles of which are assumed to mirror those of FRACKiT. However, improved stress equations have now been developed.

A stress vs. strain plot is produced from the test results. This provides both peak strength parameters and stiffness behaviour of the rock. The tensile nature of the failure can be calibrated against compressive strength (e.g. UCS test) or tensile strength (e.g. Brazilian Disc test) using comparison with standard tests or statistically from databases for the rock type concerned. The principal components of the new FRACKiT apparatus are shown in Figure 24. Details of the new FRACKiT probe are shown in Figure 25 and 26.
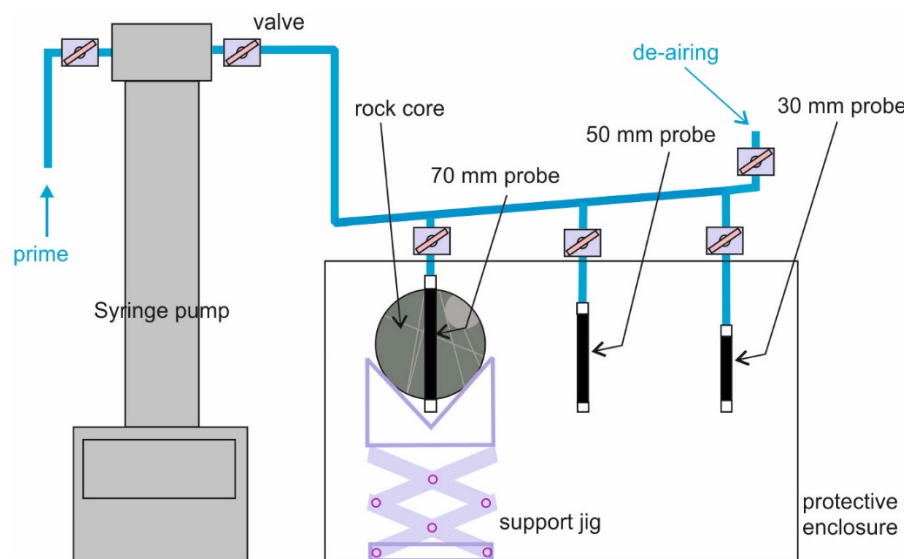
Figure 24 Schematic diagram of FRACKiT indirect tensile test apparatus
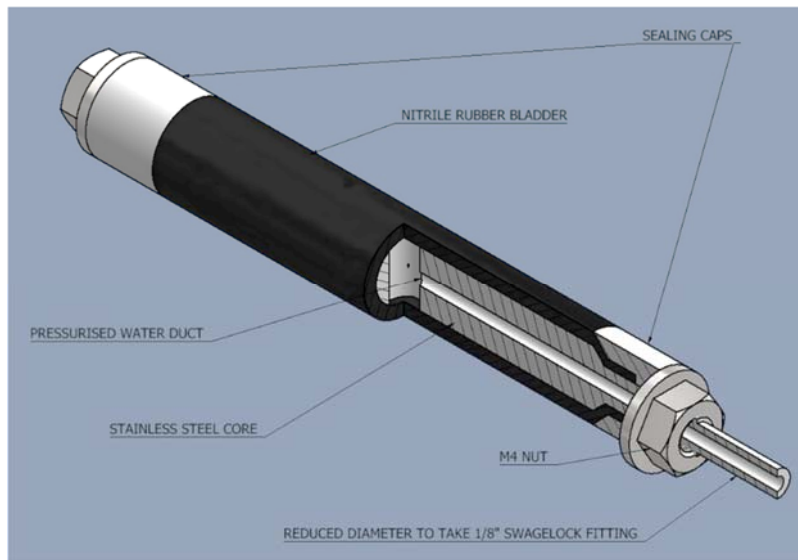
Figure 25 Cut-away schematic diagram of FRACKiT probe (10 mm diameter)

Figure 26 Location of FRACKiT probe in hole in test specimen
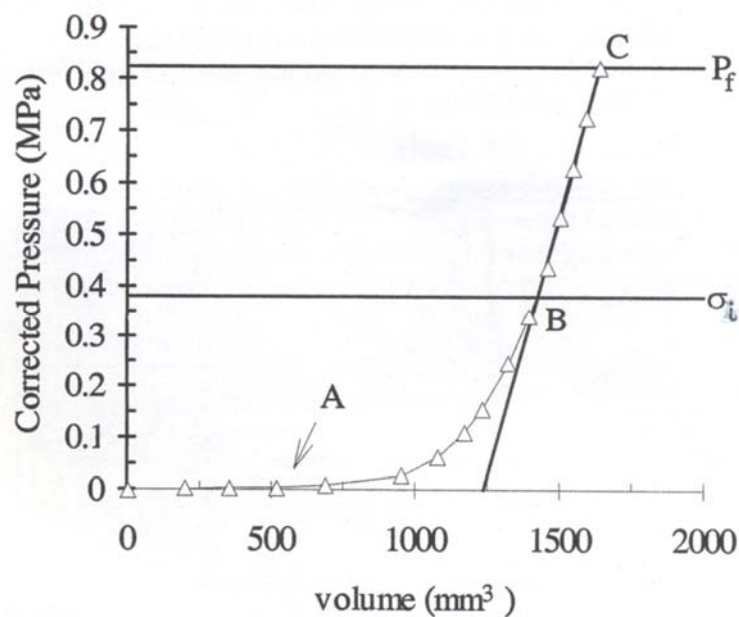
Figure 27 Plot of pressure (corrected) vs. volume for an artificial rock specimen (plaster + sand)

The assumptions regarding the stress state during a test are shown in Figure 27. The calculation of tensile strength is based on:

1. Calculation of stress, and hence tensile force, developed within the drilled diametral hole by Integration of an element of surface area (dA) of the hole subject to stress increase, produced by the inflating bladder, having a tensile component perpendicular to the plane of fracture (i.e. direction F in Figure 26).

2. Calculation of the tensile stress on the cross-section of the specimen produced by the force applied by the bladder and calculated in step 1.
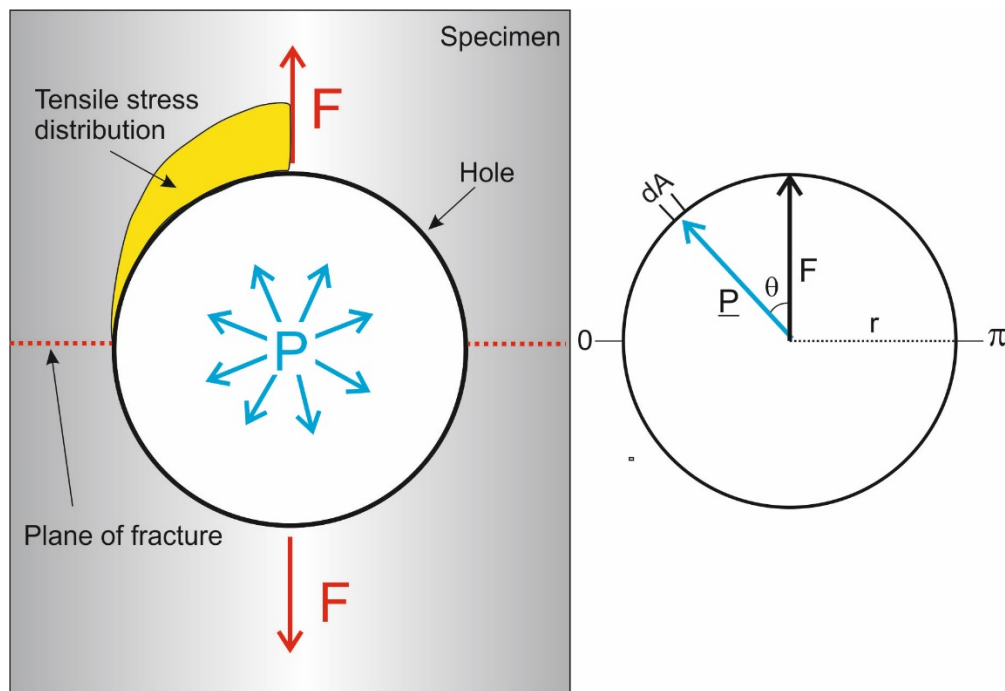
Figure 28 Schematic diagrams of the tensile stress distribution (yellow) and tensile force (F) acting parallel with the specimen axis in the drilled diametral hole resulting from stress (P) produced by inflation of the bladder (not to scale).
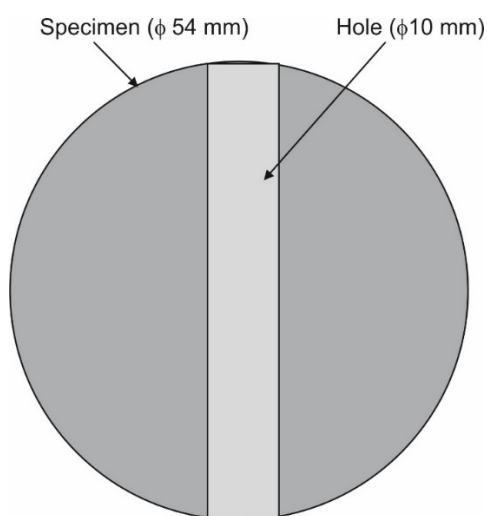
Figure 29 **Diametral cross-section of specimen and drilled hole (not to scale)**

NOTE: Cross-sectional area of the specimen's failure surface, A_f, shown as dark grey

Area element of hole:

$$d\underline{A} = L\,r\,d\theta$$

Tensile force, F

25

$$F = 2 \int_0^{\frac{1}{2}} \underline{P} \, d\underline{A}$$

Pressure, P

$$\underline{P} = |P| \cos \theta$$

where: L = length of hole, r = radius of hole, dA = area element of hole, θ = angle of force element from axial

$$F = 2 \, L \, r \, |\underline{P}| \int_{-\frac{\pi}{2}}^{+\frac{\pi}{2}} \cos \theta$$

$$F = 2 \, L \, r \, |\underline{P}| [\sin \theta] \, {}_{-\frac{\pi}{2}}^{+\frac{\pi}{2}}$$

$$F = 2 \, L \, r \, |\underline{P}| \left(\sin \frac{\pi}{2} + \sin \frac{\pi}{2} \right)$$

$$F = 4Lr|\underline{P}| \qquad\qquad (1)$$

Then:

$$P_f = \frac{F_f}{A_f} \qquad\qquad (2)$$

Where:

$$A_f = A_c - A_h \qquad\qquad (3)$$

where: P_f= Pressure at failure, F_f = Tensile force at failure, A_f=Cross-sectional area of specimen's failure surface, A_c = Cross-sectional area of specimen, A_h = axial cross-sectional area of drilled hole.

The cross-section of the failure surface, may be considered in an ideal scenario (as shown in figures 28 and 29), to be circular, as produced by a perfect planar fracture at 90º to the specimen's axis. However, in practice this surface may be elliptical, as produced by a fracture surface at an angle <90º to the specimen's axis. Despite the fact that fracture surfaces are rarely planar, a reasonable estimate of its area can be made by measuring the minimum (r_1) and maximum (r_2) radii of the ellipse resulting from fracture and using the following formula:

$$A_c = \pi \, r_1 \, r_2$$

This value can then by inserted into equation (3) above.

The apparatus provides in-hole stress by pressurising de-aired, distilled water using a Teledyne ISCO syringe pump (D-series, 100-DM) fitted with 1/8th inch and 1/16th inch stainless lines. This pump is capable of delivering at a very low rate of 0.00001 ml/min and up to 30 ml/min at pressures of up to 10,000 psi (69.5 MPa) pressure and has a fluid capacity of 103 ml.

An example of the 78 mm diameter core from the Crimple Beck borehole is shown in Figure 30. This had previously been slabbed. The condition of the core was such that breakage had occurred along multiple bedding surfaces. From this core individual pieces were trimmed for point load testing using a Metprep Brillant 200 diamond saw.

Figure 30 Sample from Crimple Beck borehole (78 mm diameter, slabbed)

Initial testing has proven that FRACKiT works in plaster of Paris. Testing will begin in shale material from the BGS archive material.

5.2.3   Initial observations of the geotechnical properties of Bowland shale

The geotechnical laboratory test programme of strength index testing of based on the Point Load Strength Index test for samples from the Crimple Beck and Cow Ark 7 boreholes has given indications of the strength classification for parts of the borehole sequences within the Bowland Shale Formation. Relationships between axial and diametral for cylindrical specimens from Cow Ark 7 and between perpendicular and parallel (to bedding) for irregular specimens from Crimple Beck have allowed strength anisotropy to be investigated and estimates of equivalent Uniaxial Compressive Strength (UCS) and Indirect Tensile Strength (ITS) to be made using published relationships for rocks in general and more specifically for mudstones and shales.

In terms of the Equivalent UCS parameter (using the ×12 factor applied to the PLSI results rather than the more familiar ×24 factor) the Bowland Shales tested fell into the strength classification 'weak' to 'very strong' with an average of 'medium strong' for Crimple Beck (perpendicular to bedding) and 'very weak' to 'very strong' with an average of 'weak' for Crimple Beck (parallel to bedding). For Cow Ark 7 the axial results gave 'weak' to 'strong' with an average of 'medium strong' and the diametral results gave 'very weak' to 'very strong' with an average of 'medium strong'.

5.2.4   Future activities

The relationship between the Point Load Strength Index test (PLSI) and the Uniaxial Compressive Strength (UCS) and Indirect Tensile Strength (ITS) tests will be investigated further for the Bowland Shale Formation. For ITS the test normally chosen is the Brazilian Disc test. This test has internationally recognised standards or recommended procedures but usually requires machining of the test specimen. The FRACKiT test provides a new method of measuring ITS with core samples in the range 'extremely weak' to 'weak', a range hitherto poorly catered for, given the difficulties in machining many types of weak rock in this category. The results described above will be linked with the observed stratigraphy.

5.3   WP4.2 TRANSPORT PROPERTIES

The recoverability of gas/oil from Bowland shale will be controlled by a number of factors, including the number and distribution of fractures, as well as the permeability of the fractured

rock. Movement of gases through shale will occur by the combined processes of molecular diffusion (governed by Fick's Law) and bulk advection. The hydraulic stimulation of shale results in the release of gas through a number of mechanisms. The fracturing of carbonate rich units, which generally have a high porosity filled will trapped gas results in direct extraction of free gas. Within the tighter, clay-rich units within the sequence, free gas is less prevalent. Some gas may be present within in-filled fractures. However, the majority of gas will either be trapped within the disconnected pore spaces of the rock, or will be sorbed onto mineral surfaces. Hydraulic stimulation will result in the formation of new fractures and will alter the stress state within the shale. A change in pressure gradient may be sufficient to initiate advective gas flow. It will also create a chemical gradient, which may promote diffusive gas flow.

In order to determine the amount of gas recoverability within a shale it is vital to understand the baseline transport properties of the intact and fractured shale. This work package will investigate these fundamental properties of flow within low permeability shale samples.

5.3.1 WP4.2.1 and WP4.2.2 Advective and diffusive flow of methane in Bowland shale

A sample of Bowland core, designated BOW-1, has been prepared from stream bed derived material collected from Lancashire, Figure 31. The sample was placed within a single closure pressure vessel applying an initial isotropic confining stress of 10 MPa. Injection and backpressures were set to 1.0 MPa respectively and the sample allowed to slowly hydrate with a synthetic brine solution prepared to mirror likely *in situ* conditions. During this time, flux into the specimen was monitored to provide data on the resaturation of the clay (Figure 32). Simultaneously, changes in the hydraulic volume of the confining system were also monitored to provide an estimate for the volume change of the specimen during hydration.

Examination of the data in Figure 32 clearly shows that at the onset of testing, a rapid uptake of water by the specimen is observed as the sample resaturates. This flux progressively declines with time, such that by around 12 days, the net flow of water into the specimen is practically zero. A similar, but less prominent response is also observed by the confining pressure pump, which indicates a small decrease in sample volume as the confining stress is applied to the core. Comparison of the cumulative flow curves from the backpressure and confining systems indicate average changes in volume of around 1.12 ml and 0.07 ml respectively, suggesting some degree of desaturation at the onset of testing. This is support by the apparent reduction in sample volume which may stem from micro-crack closure.

Once this initial equilibration stage was complete a single-step consolidation test was performed to obtain an estimate for the drained bulk modulus of the sample. Confining stress was increased to 15.0 MPa while outflow and confining system volume data were collected, with the latter equating to volumetric strain, Figure 32. Unlike other 'intact' mudrock samples previously tested, inspection of the data from BOW-1 exhibits a shorted lived transient response suggestive of microcrack closure rather than time dependent drainage. Estimates for bulk modulus, B, can be derived from the simple equation

$$B = -V\frac{dP}{dV}$$

where V is the initial volume and dP and dV are the change in pressure and sample volume respectively. In this way values for B range from 1.6 GPa (based on analysis of data derived from the confining system) to 1.9 to 3.7 GPa (for data based on fluid displaced). Given the bulk modulus of water is 2.2 GPa, it suggests much, if not all, of the interconnected porosity was saturated at the start of the consolidation stage.
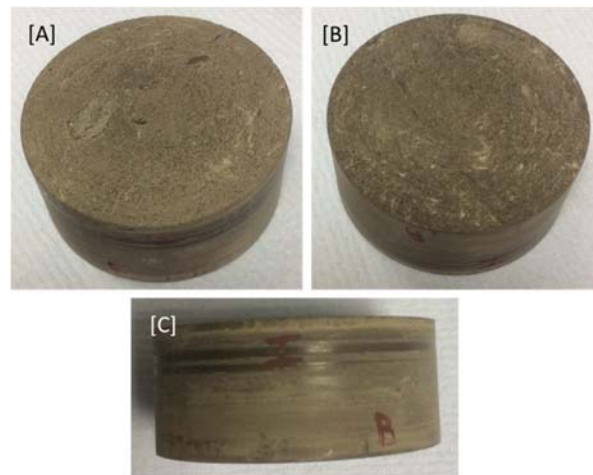
Figure 31 Photo of Bowland sample BOW-1, showing [A] injection face, [B[backpressure (downstream) face and [C] side view of core, the letters I and B denote injection and backpressure ends of the core.
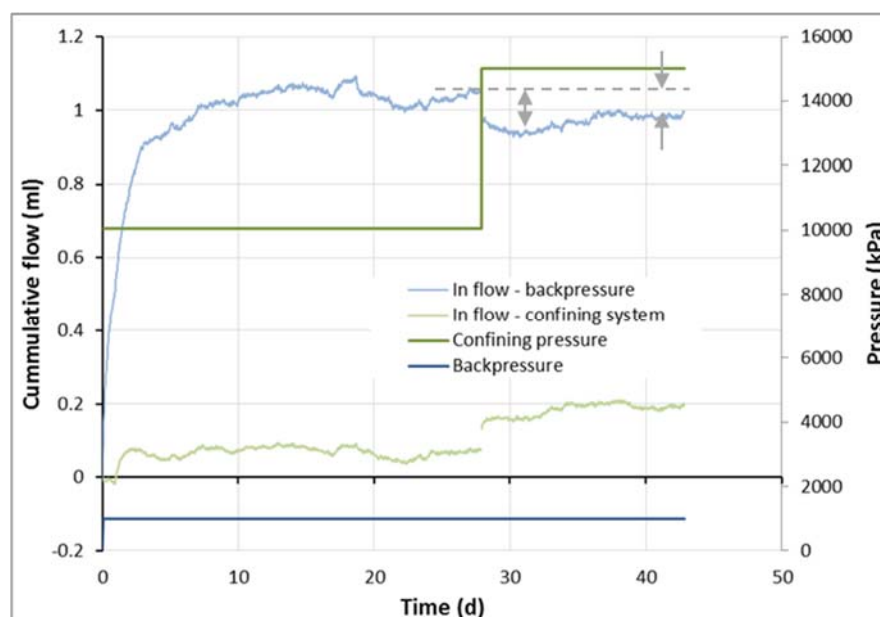
Figure 32 Cumulative flow response for backpressure and confining circuits during the initial the equilibration stage from day 0 to 28 used to resaturate the sample. Positive inflow represents flux into the specimen, with positive flow for the confining response indicative of a reduction in sample volume. At day 28 confining pressure increased to the target value of 15.0 MPa and the compressibility of the sample estimate. Grey arrows indicate picks for compressibility values reflecting the maximum and minimum probable values for this test stage.

For the hydraulic test the confining pressure was maintained at a constant level of 15.0 MPa whilst the porewater pressure at the back pressure filter was kept at 1.0 MPa. The pressure at the injection filter was raised to 6.0 MPa for 5 days after which it was returned to 1.0 MPa. Flows at the injection and backpressure filters were monitored with time with the data presented in Figure 33.

Under steady-state conditions, the intrinsic permeability of the shale can be defined as:

$$k = \frac{Q\mu L}{AdP}$$

where Q is the volumetric flow rate (m³s⁻¹), A is the sample cross sectional area (m²), dP is the pressure difference across the sample (Pa), μ is the viscosity of the water (Pa s), and L is the sample length (m). In order to define k as a function of pressure, salinity and temperature, a number of

subroutines were combined from TOUGH2 to calculate a value of 2.226×10^{-3} Pa s. Inserting this, with the values derived from Figure 33, into equation 2, yields an average value for intrinsic permeability of 4.2×10^{-21} m^2. The permeability of the shale will ultimately control the rate of fluid loss from the fracture into the matrix. Further measurements are required to better understand the temporal and spatial variability of this parameter to allow its inclusion in numerical models to predict fluid leak-off.
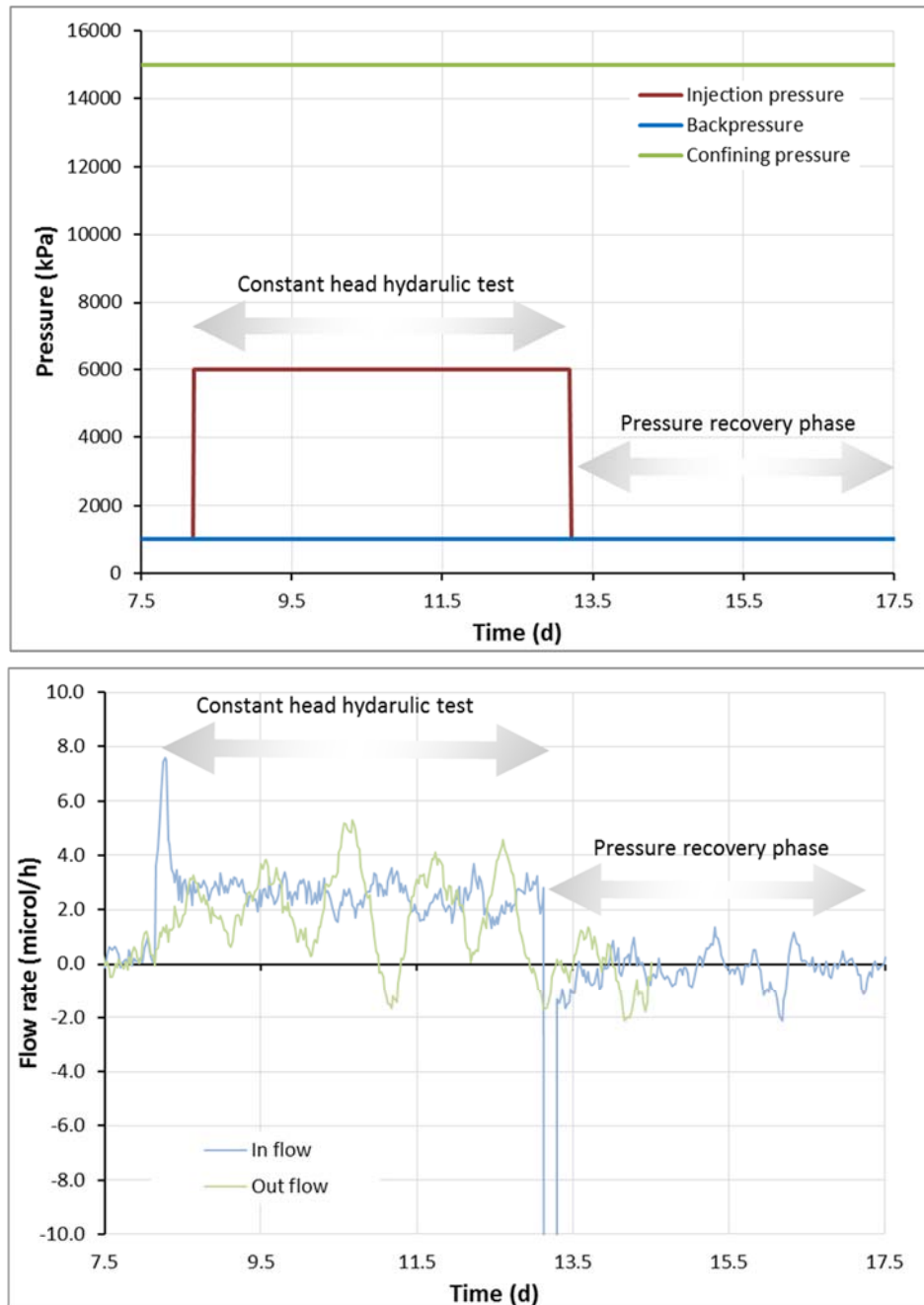
Figure 33 The first graph shows the injection, backpressure and confining pressure values during hydraulic testing to define the intrinsic permeability value of the sample. The second graph shows flow rate in and out of specimen during this phase of testing. While there is some noise in the data the steady state flow rate is clearly observed where flux in and out of the sample are approximately equal.
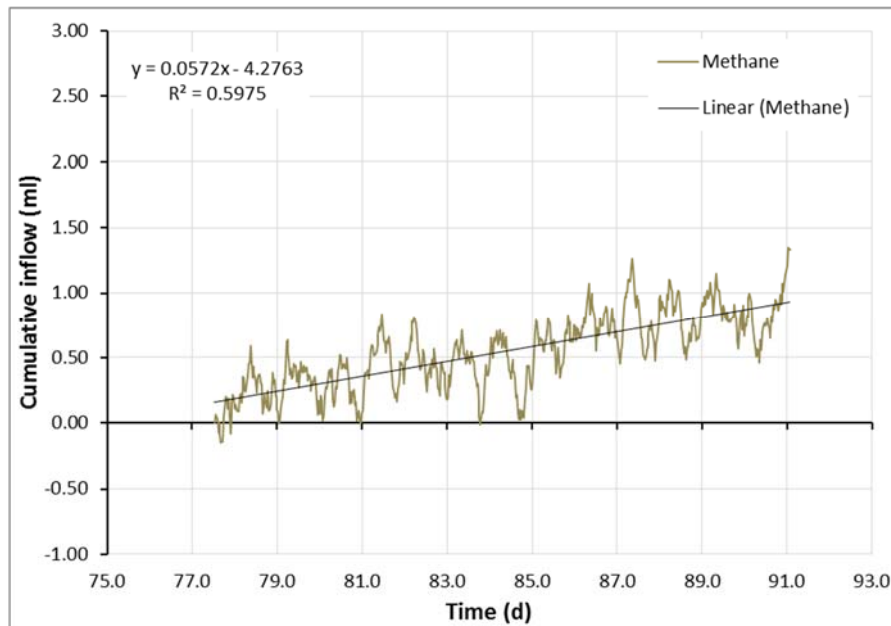
Figure 34 Cumulative CH_4 flow into sample BOW-1 under steady state conditions.

At this point in the test programme, it was decided to try and measure the steady state diffusion coefficient of methane (CH_4) through the Bowland sample. To measure this parameter, methane was introduced into a second interface vessel at a constant gas pressure of 1.0 MPa, controlled by a separate injection pump. The methane gas was allowed to equilibrate with the pump fluid (in this case brine) prior to the onset of testing. This ensured the system was both leak-tight and the pump fluids were fully saturated with methane before testing began. Once complete, the injection pump was connected to the sample and the intervening porewater flushed from the tube work to leave C H_4 in contact with the injection face of the sample. Flux in and out of the system was then monitored with time to allow definition of the steady state diffusion coefficient.

The rate of transfer of CH_4 through the sample can be obtained from the slope of the response i.e. 0.0572 ml/day at a pressure of 1000 kPa above atmospheric, i.e. an absolute pressure of 9.8680 atm. By Fick's Law, the rate of transfer is given by:

$$Rate(mole/s) = \frac{AD\Delta c}{L}$$

where A is the sample area (m^2), D is the effective diffusion coefficient ($m^2.s^{-1}$), Δc is the difference in CH_4 concentration across the sample (mole/m^3), and L is the sample length (m). The rate in mole/s is obtained from the volumetric flow rate by reducing to STP and dividing by the volume of 1 mole of gas at STP (22.4 l)

$$Rate = \frac{0.0572e-3*9.8680}{86400*22.4} = 3.05e - 10 \; mole/s$$

The concentration of CH_4 in the upstream reservoir is given by Henry's Law with the Henry coefficient for CH_4 being 1.4 mole m^{-3} atm^{-1}. Thus the concentration difference across the sample is

$$\Delta c = 1.4 * 9.8680 = 13.815 \; mole/m^3$$

Since the sample area and length are 1.9633×10^{-3} m^2 and 2.4378×10^{-2} m respectively, the diffusion coefficient is calculated as:

$$D = \frac{3.05e - 10 * 2.4378e - 2}{1.96336e - 3 * 13.815} = 2.621e - 10 \; m^2/s$$

The low solubility of CH_4 compared to that of, for example, of CO_2 (i.e. 1.4 and 34 mole m^{-3} atm^{-1} respectively), can make estimation of the diffusion coefficient problematic. Indeed, inspection of the data in Figure 34 shows considered noise leading to a coefficient of determination, R^2, of only

31

0.5975. *Further measurements of D are therefore necessary to better understand if the number above represents an accurate value for the diffusion coefficient.*
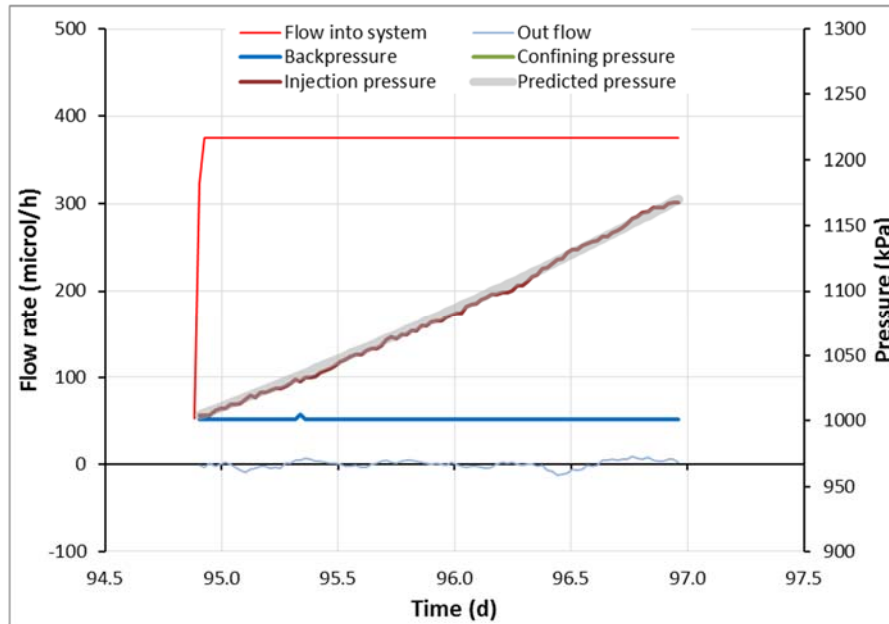
Figure 35 Gas flow rates at the injection and backpressure filters during the advective gas flow measurements. Measured, predicted and backpressure flow rates are plotted on the second y-axis.

While the diffusivity of methane may play a key role in the transfer of gas from host rock to fracture, it remains necessary to understand the processes and mechanisms governing the advective movement of gas through the Bowland shale. With this in mind, the injection pump containing the CH$_4$ was switched to constant flow rate mode, Figure 35, and the pressure slowly increased in order to obtain gas breakthrough. This phase of testing remains ongoing. Once complete the sample will be removed from the apparatus and its geotechnical properties measured.

5.3.2   WP4.2.3 Fracture transmissivity of methane in Bowland shale

Once gas is a free phase within the shale, the transport properties of the hydraulically fractures shale will dictate the yield from the shale play. This work package aims to obtain a relationship for fracture transmissivity in Bowland shale as a function of normal load.

As stated in the previous update report, sample preparation has been a considerable issue. Core material is not of sufficient size in order to produce cubic test samples. Stream-bed derived samples have also proven problematic and successful production of a test sample has not been possible. This material has a tendency to split along bedding during preparation. The successful production of a cylindrical sample for the diffusion test shows that this material can be successfully machined. Therefore a decision was made to modify the shear apparatus to use cylindrical samples, replacing the current need for cubic samples.

5.4   WP4.3 FRACTURE PROPAGATION MECHANICS

In work package 4.3 the focus is on the formation and propagation of hydraulic fractures in Bowland shale. While fracture mechanics is a mature science, the underlying physics controlling fracture formation and propagation in shale is not well described. For instance, it is currently not possible to determine whether propagating fractures simply cross lithological boundaries within a shale sequence or if they terminate where a weaker band meets a more competent one. The primary aim of the work-package is to better understand the controls on fracture formation and propagation.

5.4.1   WP4.3.1 Hydrofracturing with the laboratory

As reported in the previous update report, a scoping test was conducted using the Direct Shear Rig to prove that hydraulic fracturing was possible within the laboratory. A sample prepared from stream-bed derived material was drilled with a bore 4 mm in diameter, through which water was injected. It should be noted that the sample showed some signs of damage prior to testing, with small fractures opening along bedding planes. Initially the sample was slowly hydrated in order to seal the bore pipe through the swelling of clay material. The pore pressure was raised using a constant flow of water. Failure of the sample occurred at approximately 1.3 MPa, following which the test could not sustain any pore pressure. Figure 36 shows the resulting fracturing of the sample. As can be seen a number of fractures throughout the test were formed. This simple test proved that hydraulic fracturing at realistic in situ stresses will be possible within the laboratory.

The results from the scoping test have been used to modify the design for the Fracture Initiation Rig. The apparatus should be ready for testing by the end of Q1 of 2016.

Figure 36 Results of a pilot study to demonstrate hydraulic fracturing is possible within the laboratory. Left image shows the sample within the apparatus. The image right shows the deconstructed sample, displaying considerable fracturing of the sample.

5.4.2   WP4.3.2 Analogue hydro-fracturing study

The aim of this package of work is to directly observe the formation of fractures within Bowland shale. This will investigate influence of bedding, mineralogy, water saturation, permeant (water vs gas,), and pressurization rate on the number, distribution and volume of pathways formed.

As reported in the previous update, two initial tests were conducted on crushed Bowland shale. Figure 37 shows the results from a Fracture Visualisation test in Bowland shale. At the time of gas entry a number of fine features formed around the injection port. Following this, a number of larger fractures were formed, resulting in gas breakthrough and the escape of gas from the test. The propagation rate of the fractures was significantly greater than seen in any previous test in other clays. The loss of gas pressure was instantaneous. It can be seen that under similar conditions, the fracture network could take up to 10 minutes to form and reach breakthrough conditions in clay material. In the current test in Bowland shale, once the larger fractures started to form it took approximately 1 minute to reach breakthrough. Therefore differences are seen with the propagation rate of fractures and the release of energy once the gas started to propagate within the clay paste. This indicates that the Bowland shale was behaving as a more competent material, until gas breakthrough where fracture formation was easier. This will be investigated in greater detail in following tests.
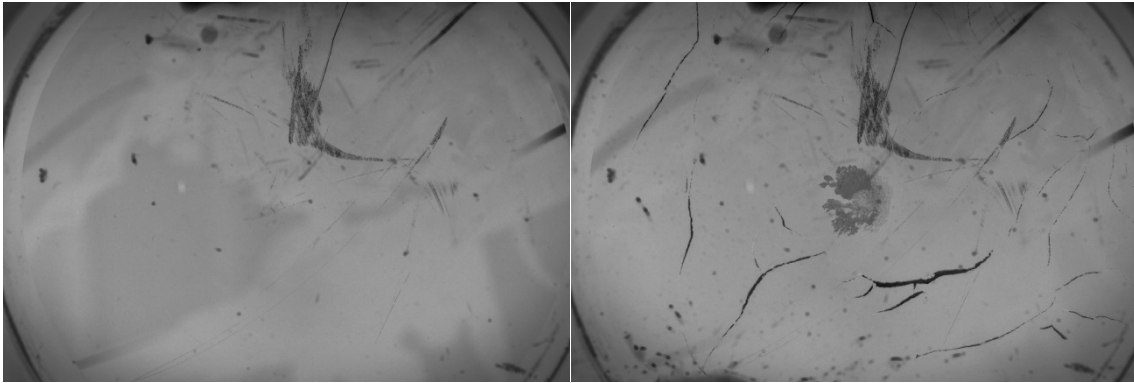
Figure 37 Results of a Fracture Visualisation test in Bowland shale. Left shows the sharting conditions (note that the glass of the FVR has become scratched). Right shows the formation of a large number of fine fractures around the injection port (centre of image) and a number of large fractures throughout the test sample.
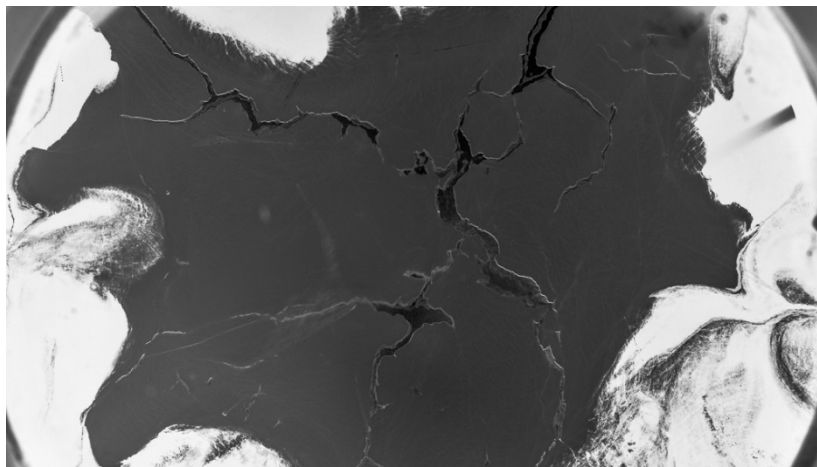
Figure 38 Results of a Fracture Visualisation test in a mixed clay system (Bowland shale and kaolinite).

Testing has moved onto looking at dual clay systems. The question to be addressed is how fractures cut boundaries between materials of distinctly different physical properties. Two scoping tests have been conducted to test our ability to produce clean boundaries between dissimilar clay pastes. Figure 38 shows that some difficulty has been encountered in creating such a clear boundary between kaolinite and crushed Bowland shale; this technique is being perfected to aim to produce as close to a circular interface as possible. However, the irregular boundary between the two clays can be seen to control fracture growth. The fractures propagate towards the boundary and can be seen to deflect. Gas breakthrough is unfortunately not observed by the time-lapse camera, but from the view we have it is possible to state that no fractures are seen to cut the boundary between the two clays. The rheology of the clays, and the way the two clays interact, controls fracture propagation. Whilst this research is early in its development, this illustrates that hydraulic fractures are likely to become bound by lithological layers and propagating fractures through lithological boundaries is likely to be difficult. These observations help to strengthen the observations of Fisher & Warpinski (2011), who noted that below a critical depth the ratio of vertical to horizontal hydro-fractures is complex; whereas classical theory would predict vertical fractures aligned with the maximum principal stress direction. Whilst the current tests have been conducted on paste material using gas as a permeant, the observations are likely to be similar in more lithified shale; this will be investigated later in the test programme.

Future testing will concentrate on conducting methane and water injection studies into crushed Bowland shale at varying water content and normal stress; as well as tests conducted on dual-clay systems. The use of two clays will be performed with a both a circular arrangement (to force cross

cutting of the clay interface) and a layered arrangement to observe whether fractures remain lithologically bound.

5.5   WP4.4 IMPACTS OF HYDRAULIC FRACTURING

Work package 4.4 will address societal questions about the consequences of hydraulic fracturing. To date, BGS has been asked two specific questions about the hazards created by hydraulic stimulation. The first is the question about waste water. Statistics from the US suggest that significant quantities of injected water are not recovered; this may be more than 50 % of the water injected. The question arises as to where this water goes, with a common assumption that this waste water must have leaked into neighbouring aquifers. The second question is about the risk of subsidence. Pressure groups in Lancashire have suggested that several metres of subsidence will occur following extraction of gas. This assumes that an unconventional hydrocarbon system behaves much the same as a conventional one. A previous BGS desk study (Cuss, pers. comm.) suggested that the dilatancy created by hydraulic fracturing may actually result in small amounts of heave (the opposite of subsidence), although as this would occur at 3 km depth it is unlikely to have any surface impact. Therefore it is necessary to investigate whether subsidence, heave, or neutrality will occur.

5.5.1   WP4.4.1 Water uptake study

This package of work will consist of two activities. The first will be a desk based study examining the osmotic efficiency and water uptake capacity of Bowland shale. This will be defined as an uptake per time per unit area. This will be combined with estimates of fracture surface area per cubic metre to estimate the uptake of water in Bowland shale. The second activity will be experimental data in support of the theoretic study. Hydraulic fracture experiments will be conducted whereby known volumes of water will be injected, known volumes will be recovered and thus water uptake will be measured. By leaving the experiment for prolonged periods of time following recovery of fluid, the uptake of water with time will be examined.

As stated for WP4.3.1 and WP4.2.3 this work package is dependent on the production of a modified apparatus that is not expected until the end of 2015 at the earliest. However, the test conducted on Bowland shale for the advective and diffusive study showed that in the early stages of testing the sample had an approximate 1 ml uptake of water. As the sample was approximately 40 ml in volume, this suggests the sample had a 2.7 % uptake of water. A caveat is required though, as the stream derived sample may not have been fully saturated and a degree of this water uptake would have been due to drying effects. The geotechnical properties for this sample will be calculated following the completion of the test and will ascertain a starting saturation. From this estimate it will be possible to determine the uptake of water of Bowland shale.

5.5.2   WP4.4.2 Subsidence vs heave study

This activity will investigate the risk of subsidence over a shale gas play. In a conventional hydrocarbon system the extraction of free gas can result in subsidence, depending on the pressure control employed by the drilling engineers. It is understandable that the public has been alerted to the possibility of gas extraction resulting in subsidence in the overlying areas. It has been suggested by pressure groups in Lancashire that several metres of subsidence will occur following extraction of gas. An unpublished simple desk study was conducted by BGS that suggested that the dilatancy created by hydraulic fracturing may actually result in small amounts of heave (the opposite of subsidence), although as this would occur at 3 km depth it is unlikely to have any surface impact. Therefore it is necessary to investigate whether subsidence, heave, or neutrality will occur.

As stated for WP4.3.1 and WP4.2.3 this work package is dependent on the production of a modified apparatus that is underway.

5.6   CURRENT STATUS/FUTURE OPTIONS

Work package	Title	Current status	Deliverable
WP4.1.1	Strength	Sample selection has been completed. Testing has been completed for point load testing, uniaxial compressive tests and Brazilian tests will commence soon.	Report and paper in 2017
WP4.1.2	FRACiT	Apparatus has been completed. Initial testing is promising. Test programme on Bowland shale will begin shortly. Full comparison with existing geotechnical techniques will be undertaken.	Paper in 2017
WP4.2.1	Advective flow	Initial test using stream bed material is currently on-going. Detailed test on Roosecote material to begin early in 2016.	Paper on flow in Bowland Shale
WP4.2.2	Diffusive flow	Completed	
WP4.2.3	Fracture flow	Awaiting modification of apparatus. To begin in early 2017.	
WP4.3.1	Fracking	Awaiting apparatus manufacture. To begin in early 2016.	Report
WP4.3.2	Analogue	Test programme on-going.	
WP4.4.1	Water	Awaiting modification of apparatus. To begin in early 2017.	Report
WP4.4.2	Subsidence	Awaiting modification of apparatus. To begin in early 2017.	

Appendix 1   Details of outcrop samples reported in section 4

Collectors Number		Original sample type	1:50 k map sheet (geol)	NGR 100 km square	Easting	Northing	Sample elevation/ depth	Location Information (words related to info on 50k sheet)	Geological Description (comment on field relations)	Lithology	Chronost rat code	Lithostrat code
RBH	1064	bulk	99	SK	410255	385186	270	102m south of phone box at Upper Booth along stream stream bank	Dark fissile mudstone with gradational top in lowest part of logged section. Contains large squashed calcareous bullions.	Mudstone, calcareous	E2b	BSG
RBH	1065	bulk	99	SK	410255	385186	270	102m south of phone box at Upper Booth along stream stream bank	Very thin bedded, calcareouse, dark grey with fairly sharp base. Lenticular calcareous zones. Small goniatite seen. Approximatly 2m from base of logged section	Mudstone, calcareous	E2b	BSG
RBH	1067	bulk	99	SK	409566	385531	300	100m west of Lee House west of Upper Booth	Dark grey, very hard ferugenous mudstone with slight carbanate and goniatite. SAMPLE RBH043 - bullion	Mudstone, calcareous	R1a1	BSG
RBH	1068	bulk	99	SK	409566	385531	300	100m west of Lee House west of Upper Booth	Dark grey, very ferrugenous, finely laminated with pockets with abundant goniatite. SAMPLE RBH044 - shale	Mudstone, black organic	R1a1	BSG
RBH	1069	bulk/fossil	99	SK	409566	385531	300	100m west of Lee House west of Upper Booth	SAMPLE RBH045 Abundant fossils. Soft claystone. Looks paler in weathered section. Less fissile	Mudstone, black organic	R1a1	BSG
RBH	1070	bulk	99	SK	410260	385476	278	190m north of phone box at Upper Booth along stream stream bank	Medium dark fissile mudstone. Soft. SAMPLE RBH046 approximatly 2m above base of section.	Mudstone, black organic	H1a1	BSG
RBH	1071	bulk	99	SK	410278	385610	288	323m north of phone box at Upper Booth along stream stream bank	Med grey to dark grey, fissile, mudstone. At the base in the stream where sampled there is a harder feruginous bed.	Mudstone with common ironstone	H1b	BSG
RBH	1072	bulk	99	SK	410978	384783	245	43m west of the railroad bridge crossing the River Noe near Barber Booth	Malamense Marine Band - thick sucsession of calcareous mudstones with abundant brachs	Mudstone, calcareous	E1c1	BSG
RBH	1073	bulk/fossil	59	SD	364469	453466	280	652m west southwest of Lower Brennand in Hind Clough	Full of delicate ?brachiopods traces. Ferugenous, medium dark grey, concoidal breaking. Very thinly bedded. Firm. Sharp top. Better cemented Than lower unit. Calcareous.	Mudstone, calcareous	P2c	BSG
RBH	1075	fossil	60	SD	372166	457221	198	251m west of the confluence of the River Hodder and Hasgill Beck	Small section of muddy limestones and mudstones.	Mudstone, calcareous	P2b	BSG
RBH	1076	bulk	67	SD	359213.6902	444981.6734	320	624m northeast of Blindhurst	E. pseudobilingue MB (lower)	Mudstone, calcareous	E1b2	BSG
RBH	1078	bulk	67	SD	359213.6902	444981.6734	330	624m northeast of Blindhurst	E. pseudobilingue MB (upper)	Mudstone, calcareous	E1b2	BSG
RBH	1080	bulk	68	SD	372707	435356	108	801m SSW of Abby at Whalley	Calcareous Mudstone C. malhamense MB	Mudstone, calcareous	E1c1	BSG
RBH	1081	bulk	68	SD	372688	435374	100	795m SSW of Abby at Whalley	Micaceous mudstone near ?E. Pseudobilingue	Mudstone, black organic	E1b2	BSG
RBH	1082	bulk	68	SD	375156	437628	173	In stream 705m NE of PH at Wiswell	Calcareous Mudstone near C. Leon MB	Mudstone, calcareous	E1a1	BSG
RBH	1083	bulk	68	SD	375211	437560	190	In stream 734m NE of PH at Wiswell	Black Mudstone	Mudstone, black organic	E1b2	BSG
RBH	1084	limestone	68	SD	374921	437453	153	In stream 415m WSW of PH at Wiswell	Calcareous mudstone near S. splendens MB	Mudstone, calcareous	P2	BSG
RBH	1086	fossil	68	SD	383238	444270	248	In steam 603m ENE of Higher Gills	Goniotite	Mudstone, calcareous	P1a	BSG
RBH	1088	bulk	68	SD	383231	444112	265	In stream 569m east of Higher Gills	Mudstone below first sandstone of Pendleside Sandstone	Mudstone, black organic	P1a	BSG
RBH	1089	bulk	68	SD	385923	444973	365	In stream 250m NE Weets Hill	Mudstone	Mudstone, black organic	E1c1	BSG
RBH	1090	bulk	68	SD	385923	444973	365	In stream 250m NE Weets Hill	Mudstone	Mudstone, black organic	E1c1	BSG
RBH	1091	bulk	69	SD	397895	449183	125	In stream 371m west of Butler Hill	Mudstone	Mudstone, calcareous	E1	BSG
RBH	*1092*	*limestone*	*60*	*SD*	*384464*	*462377*	*330*	*In stream 423m ESE of Scaleber Force*	*Mudstone*	*Mudstone, calcareous*	*P2*	*BSG*
RBH	1096	bulk	60	SD	384986	458750	210	In stream 838m NNW of Little Newton	Fossiliferous mudstone	Mudstone, black organic	E1	BSG
RBH	1097	bulk	60	SD	385026	458674	208	In stream 748m NNW of Little Newton	Fossiliferous mudstone	Mudstone, calcareous	P2	BSG
RBH	1098	bulk	60	SD	385031	458654	206	In stream 710m NNW of Little Newton	Mudstone	Mudstone, calcareous	P2	BSG

37

Appendix 2   Experimental Investigation of the Fluid-Rock Reactions of Bowland Shale Experimental Investigation of the Fluid-Rock Reactions of Bowland Shale
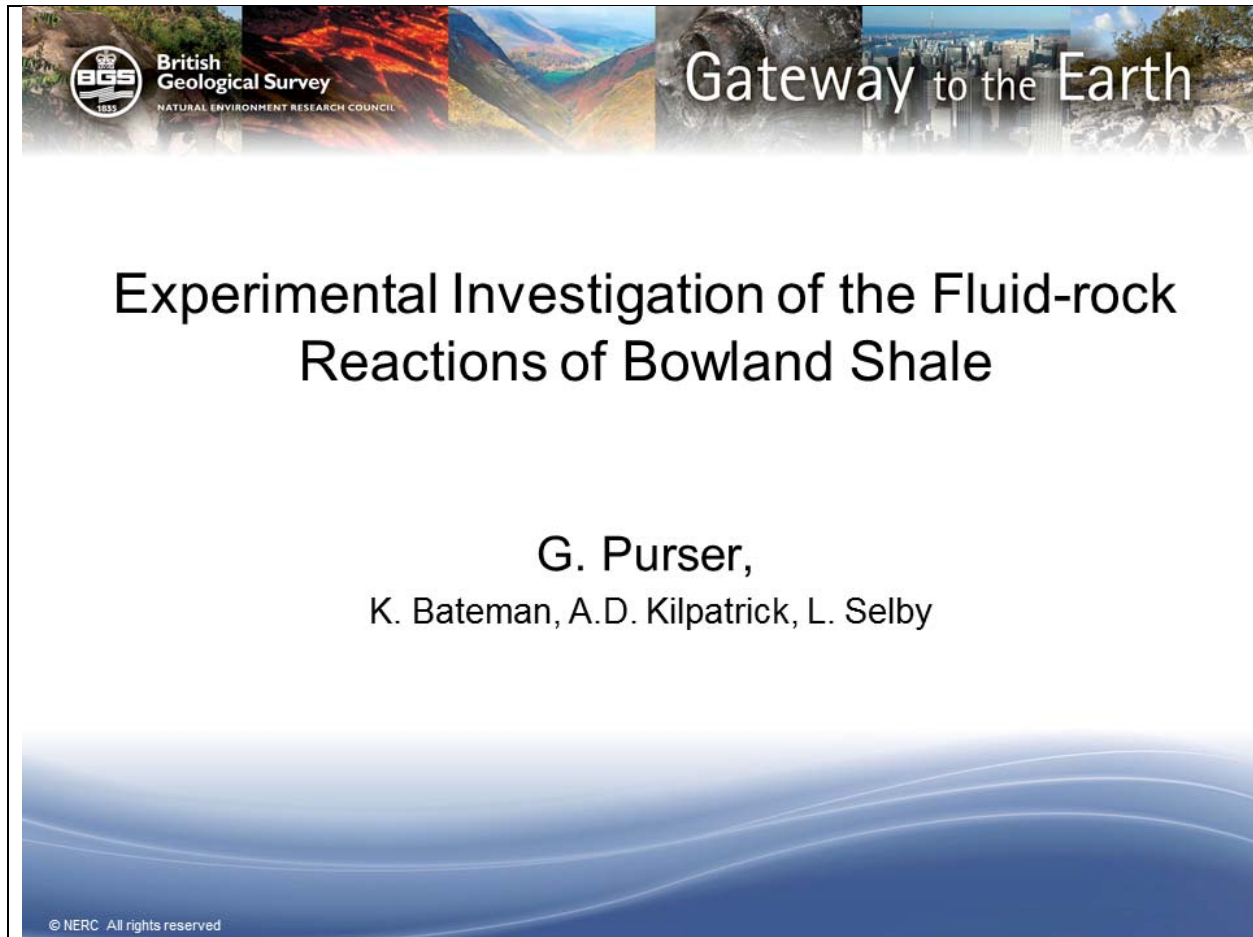
Aims

- Determine which components in shale may become mobilised under conditions relevant to shale gas exploitation.
- Determine the rate at which they are dissolved and their likely maximum concentration.
- Identify mechanisms that might naturally limit the concentration of these dissolved components.

How:

- Following fluid chemical evolution within batch experiments involving samples of shale in contact with fluid.
- Speciation and mineral equilibrium modelling
  - degree of saturation of the fluids
  - What secondary phases might precipitate

Experiments

N$_2$ Gas
150 bar Fluid Out

N$_2$ Gas

Injection fluid (Tapwater)

Crushed shale

Sample tube

Filter

Magnetic stirrer
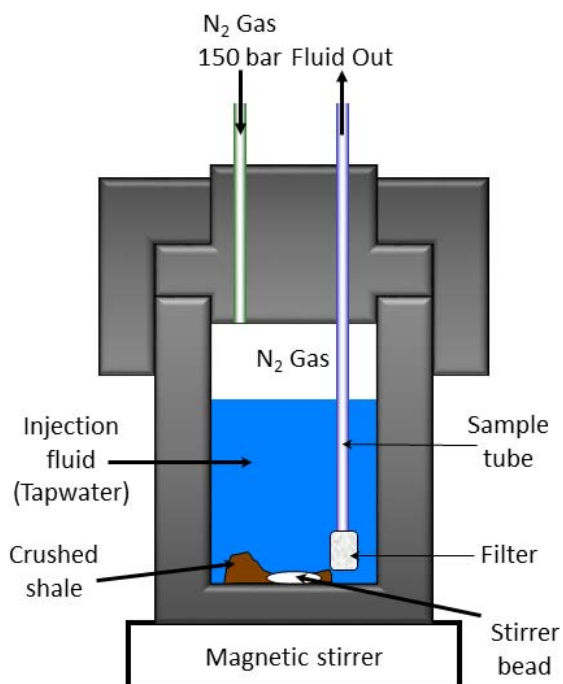
Stirrer bead

Solids
- Crushed Bowland Shale
- Roosecote-1 borehole located in south Cumbria drilled in 1970-71.
- 500 µm – 2000 µm fraction

Fluid
- (Local) tap water

Conditions
- 40°C, 150 bar (N$_2$)

Fluids sampled over 6 months.

Mineralogical composition

Mineralogical composition

Borehole name	Depth (m)	Mineral %											
		Quartz	Plagioclase	K-Feldspar	Calcite	Dolomite (Ankerite)	Siderite (Ca, Mg)	Pyrite	Marcasite	Anatase	Mica	Kaolinite	Chlorite
Roosecote-1	600	60	nd	nd	9.6	2.8	nd	1.3	<0.5	nd	24.4	1.6	nd

Fluid chemistry

Fluid composition

Composition	pH	Ca	Mg	Na	K	HCO_3^-	Cl^-	SO_4^{2-}	NO_3^-	Br^-	NO_2^-	HPO_4^{2-}	Si
								$mg\ l^{-1}$					
Starting fluid	7.45	17	3	9	1	40	11	19	2	0.023	0.044	0.22	0.72
After 6 month	8.28	32	6	139	7	172	70	150	16	0.36	0.15	0.073	9

	Ba	Sr	Mn	Fe	Li	B	Al	Ti	V	Cr	Co	Ni	Cu	Zn
								$\mu g\ l^{-1}$						
Starting fluid	29	56	0	6	0	0	7	0	0	0.36	0.04	1.1	200	116
After 6 month	4	274	12	5	39	195	17	0.2	17	0.18	0.43	16	5	8

	As	Se	Rb	Mo	Ag	Cd	Sn	Sb	Cs	W	Tl	Pb	U
						$\mu g\ l^{-1}$							
Starting fluid	0	0.3	0.72	0	0	0.05	0.12	0.19	0	0	0	0.35	0.14
After 6 month	9	23	13	360	0	0.1	0	19	0.96	0.24	0.24	0.06	28

Mineral reactions
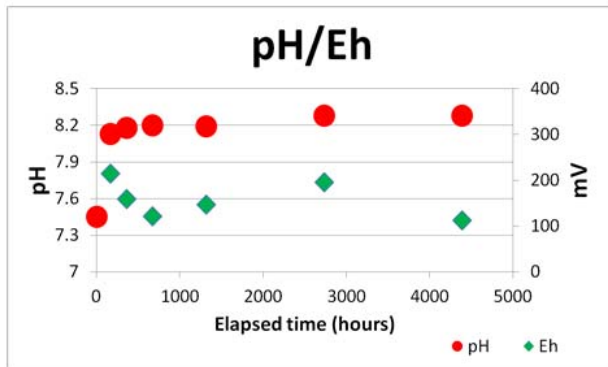
Initial decrease in Eh (redox) observed possibly due to the oxidation of pyrite found in the shale.

Overall pH increases, maybe due to the dissolution of carbonate (calcite/dolomite) minerals.

Increase in Ca and HCO_3^- initially with the dissolution of carbonates.

Possibly later some minor re-precipitation of carbonates.
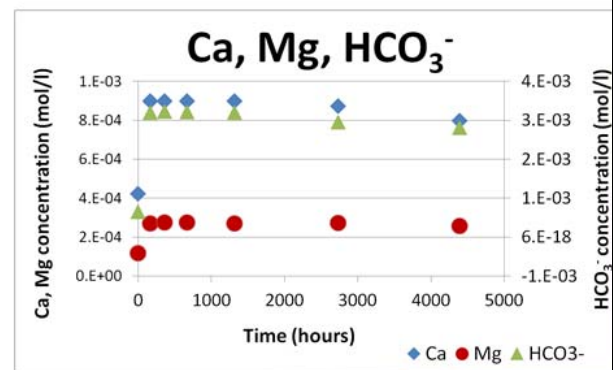
Mineral reactions
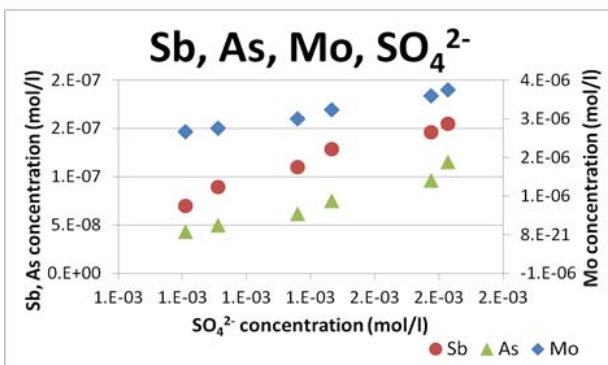
Sb, As, Mo are known impurities in pyrite and tracked the release of sulphate.

Sulphate (SO_4^{2-}) is generated during oxidation of pyrite.

Se, V, Mn, Co increase rapidly during initial experimental stage (mineral dissolution) then decreased in concentration over the 6 month experiment.
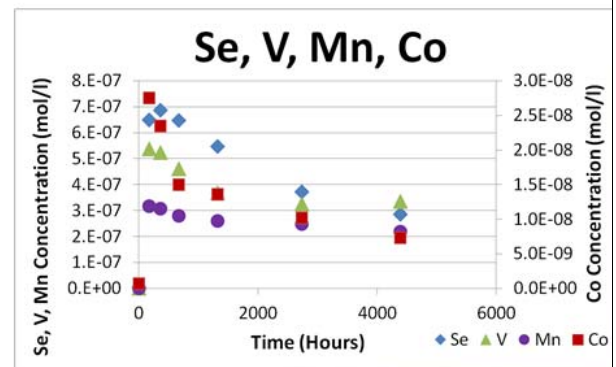
Mineral reactions
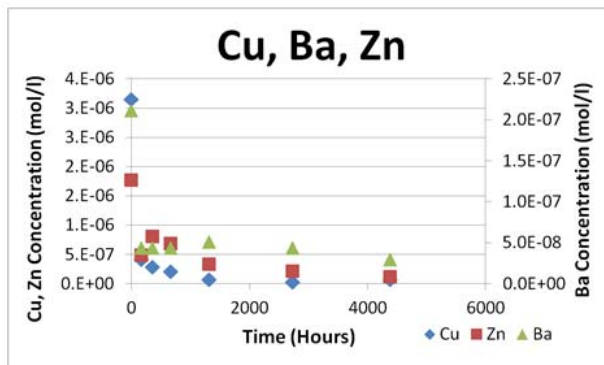
Cu, Ba, Zn

Cu, Ba, Zn were rapidly removed from the injection water.
- Possibly removed by mineral formation e.g. BaSO4.
- Or interactions with clays/metal hydroxides?

Uranium possibly released during oxidation of pyrite (as a trace impurity)

Later re-precipitated as a mineral phase or adsorbed onto surfaces during metal (iron) hydroxide formation

U
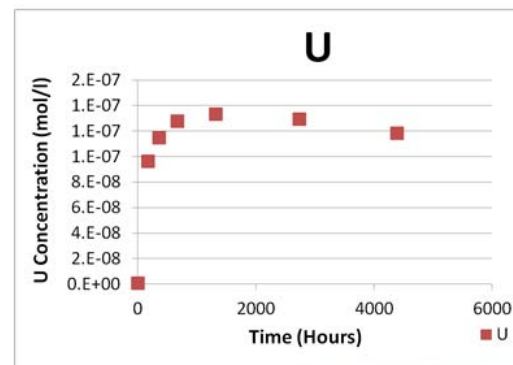
Where next?

- Experiments with fresher shale
  - ➢ Determine the organic content released
  - ➢ Mineral reactions – do they match?
  - ➢ Geochemical modelling to better understand production of iron hydroxides and clays
  - ➢ Explore possible metal adsorption/desorption on metal oxides and ion exchange in clays

- Experiments with other fracking fluids?
- Compare the experimental results with other fluids generated during field tests (Presse hall)

Appendix 3 Characterization of the kerogen fraction of Arnsbergian (late Mississippian, Serpukhovian) mudstones in the UK Pennine Basin

Introduction Project Description Take away   Results   STEM   Py-GC   Biostrat.   Conclusions

Tectonic framework for the Mississippian of Southern Britain
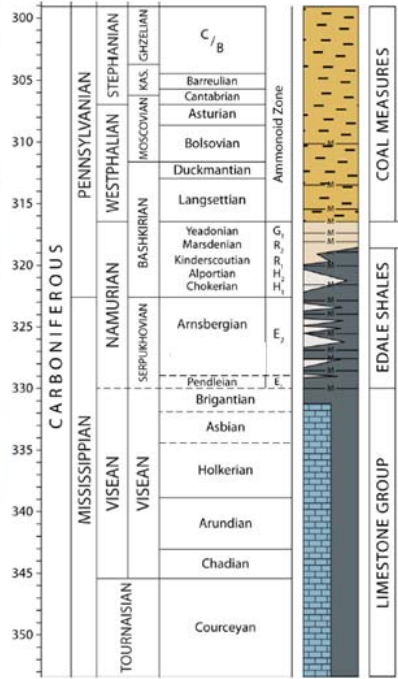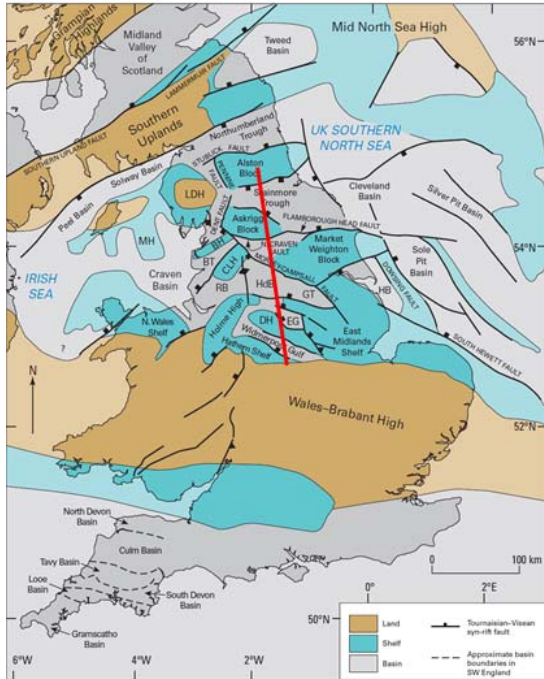
Fluvial plain deposits with distributary channel fills and thin coal horizons

Interbedded pro-delta turbiditic and mouth ba[r] sandstones

Fossiliferous mudstone[s] (marine bands): cycle[s] with sandstones

Draping of mudstones over the platforms

Deep-water mudstones and calciturbidites deposited in rapidly subsiding, fault-bounded basins

Carbonate deposition on platforms

(Aitkenhead et al., 2002; Waters and Condon, 2012)

Introduction Project Description Take away   Results   STEM   Py-GC   Biostrat.   Conclusions

Schematic Cross-section showing the main Namurian units

Rossendale Fm(G₁)
Marsden Fm(R₂)
Hebden Fm(R₁)
Samlesbury Fm(H)
Silsden Fm(E₂)
Pendleton Fm(E₁)

ASKRIGG BLOCK

DERBYSHIRE PLATFORM/ EAST MIDLANDS SHELF

Morridge Formation

ALPORT & EDALE BASINS

NORTH STAFFORDSHIRE BASIN

HOLME HIGH

WIDMERPOOL GULF

CENTRAL LANCASHIRE HIGH

BS   Bowland Shale Formation (CRAVEN GROUP)

CRAVEN BASIN

Delta top and fluviatile
Delta slope and turbidite fan   } Sandstones from northern source (Millstone Grit)
Delta slope and turbidite fan sandstones from southern source (Morridge Fm)
Limestone and chert
Mudstone
Formation boundaries
Stage boundary

(Waters et al. 2009)

© NERC All rights reserved

© NERC All rights reserved
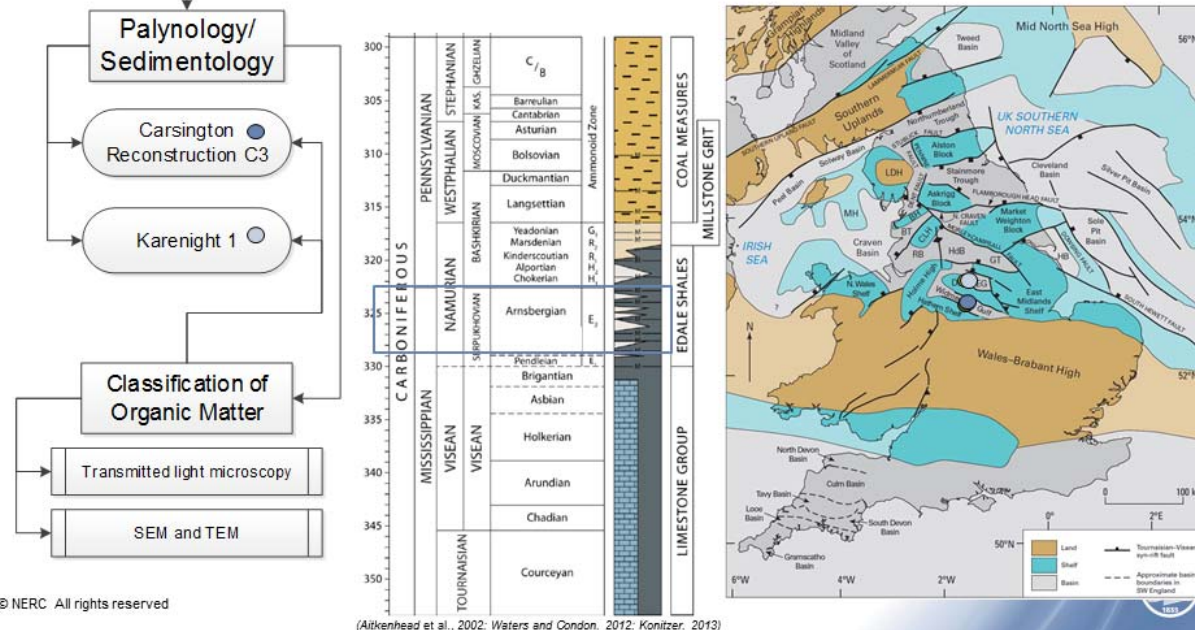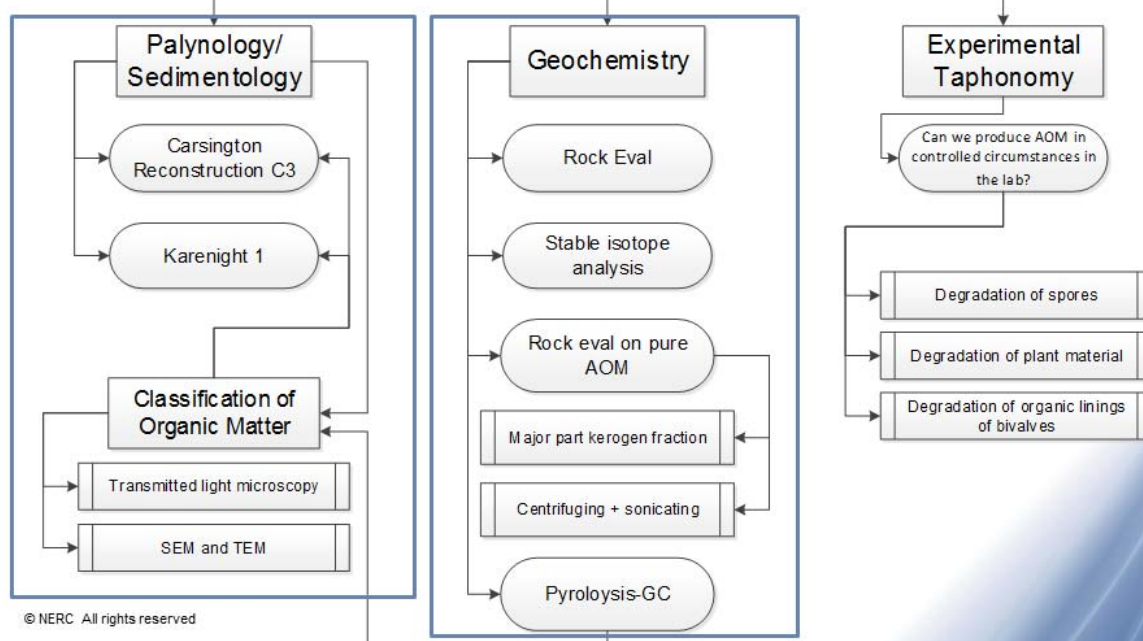
Take away message:

1) Results of the palynology/Geochem show the expected cyclicity and give an in-depth image of the depositional environment.

2) STEM analysis should make us think differently about resource estimation.

3) Results of Pyrolysis-GC: (very) targeted estimates may have to occur.

4) Spore biostratigraphy may be the key in making this very targeted approach possible.

Carsington Dam Reconstruction C3

- Calcareous mudstone

- Bivalves very common

- Relatively High TOC (3-5 %)

2 cm

- Mudstone, mostly non-calcareous

- Many sandstone intervals

- Plant fossils common

- Relatively low TOC (2%)

- Regular siderite concretions

2 cm

2 cm
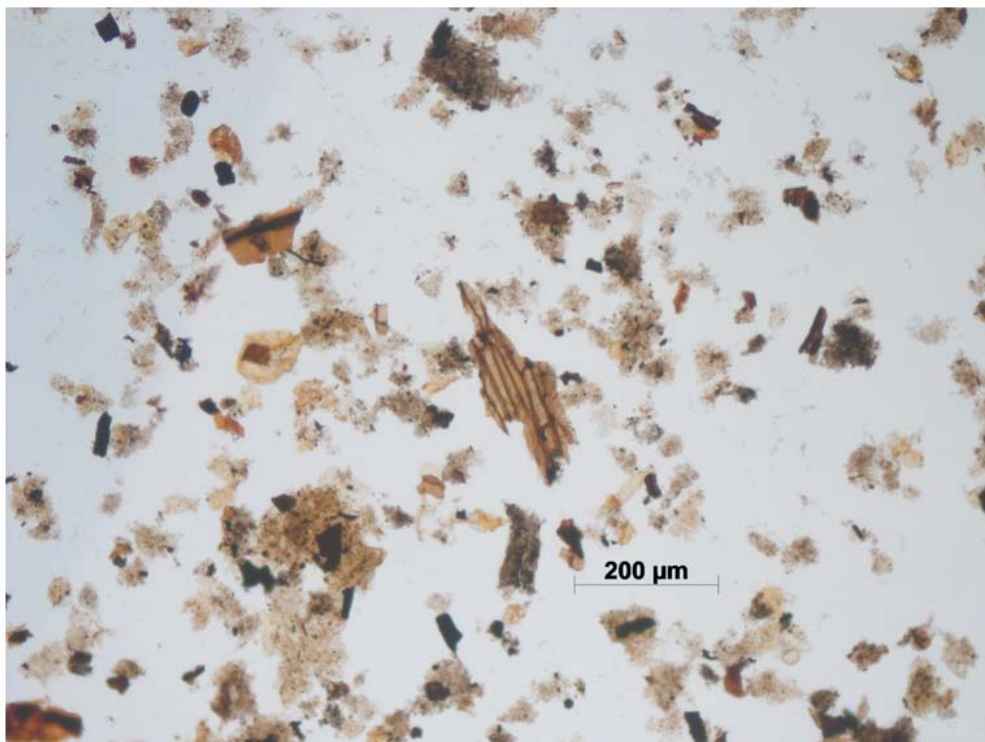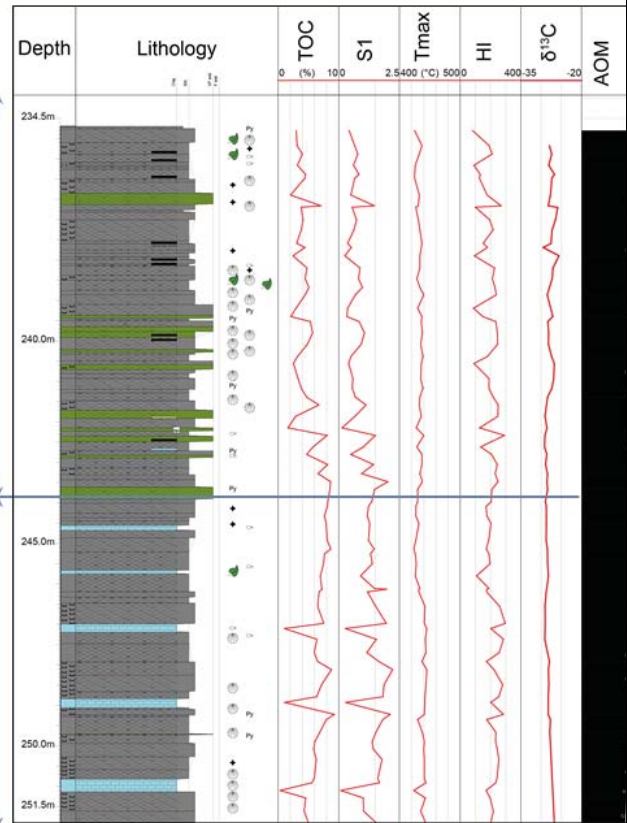
Classification of organic particles, grouped by origin

Ternary AOM–Phytoclast–Palynomorph plot

Heterogeneous AOM: pellicular Amorphous Organic Matter
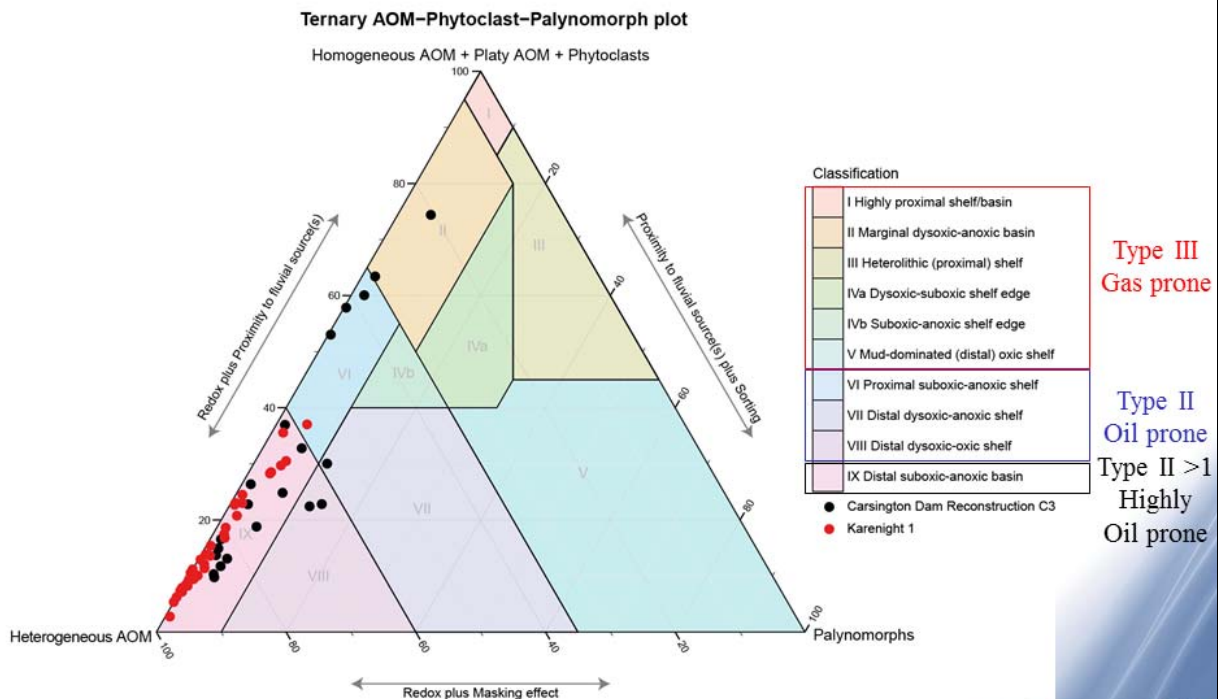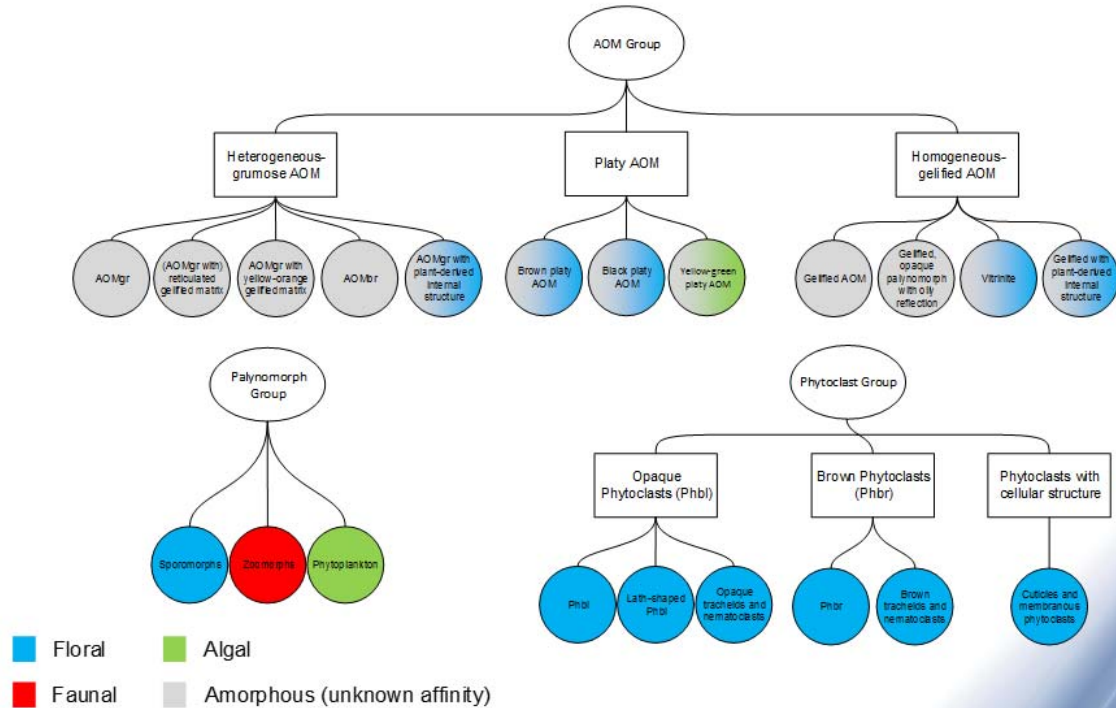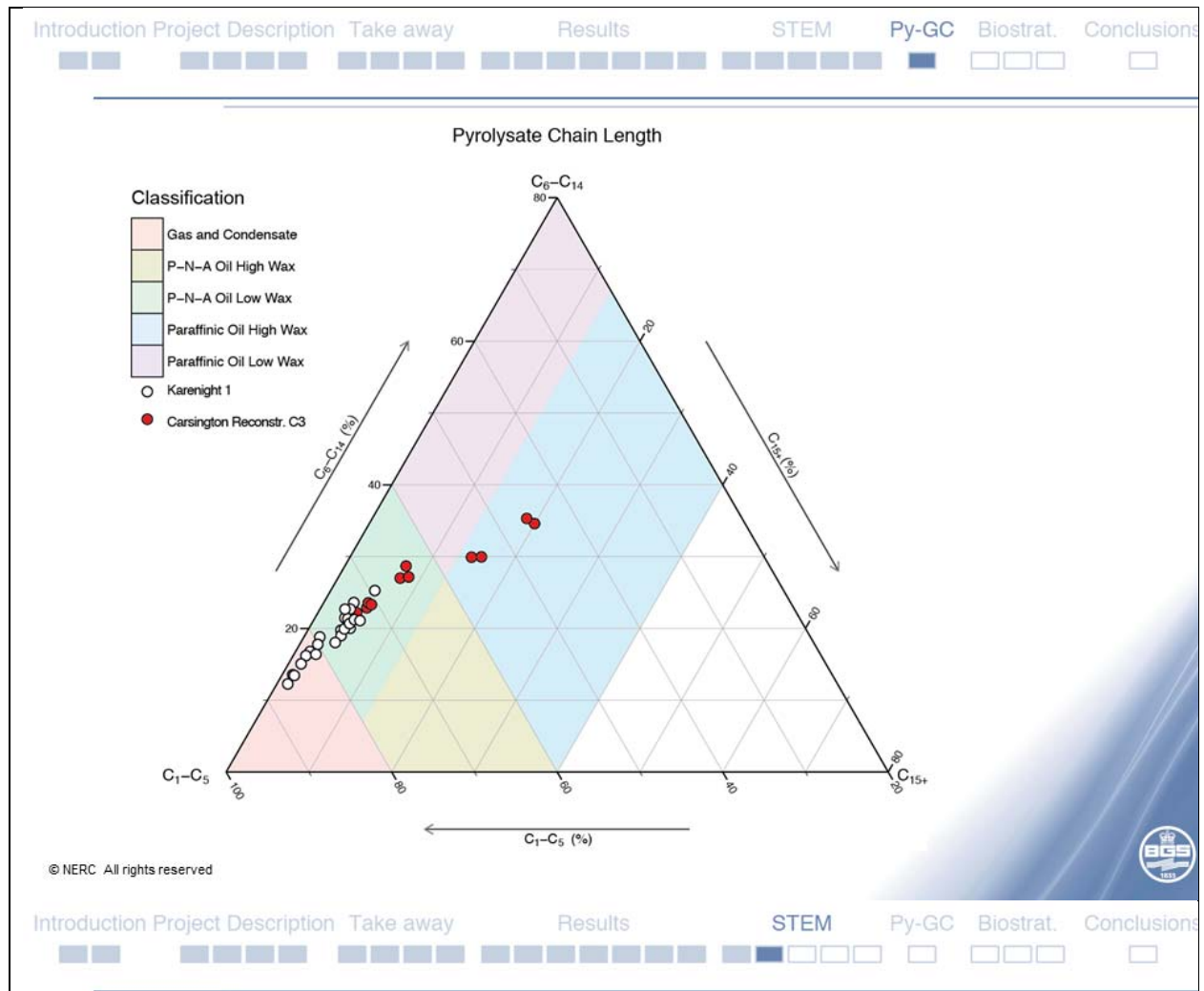
Heterogeneous AOM: pellicular Amorphous Organic Matter
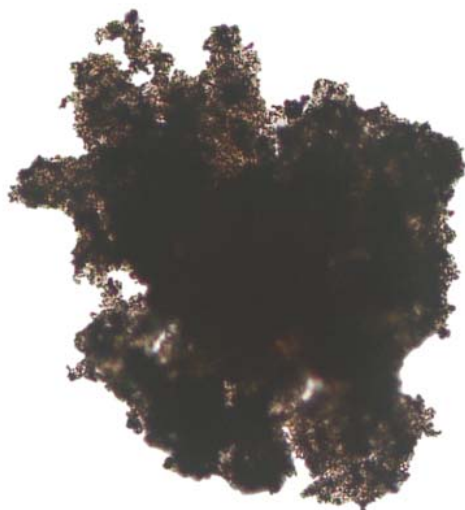
50 µm

curr	HV	det	WD	vacMode	10 µm
0.68 nA	30.00 kV	STEM	14.9 mm	High vacuum	JH021
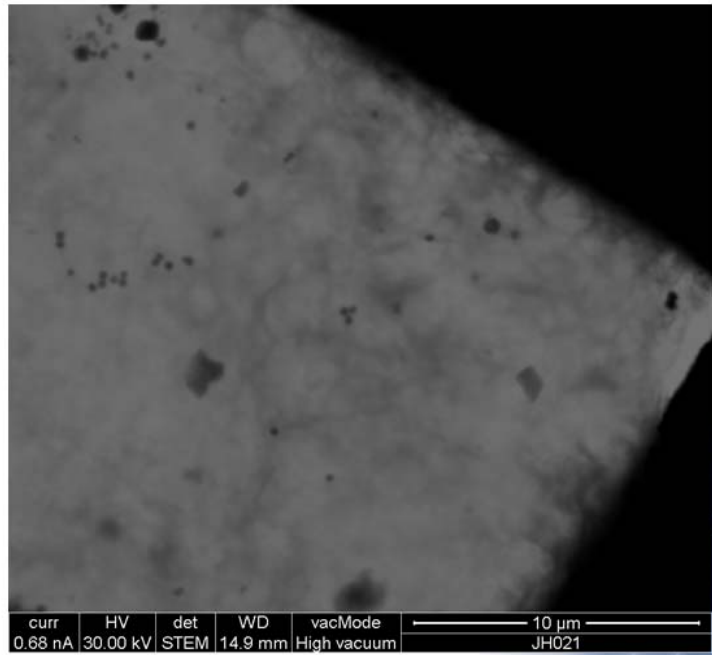
Black phytoclast
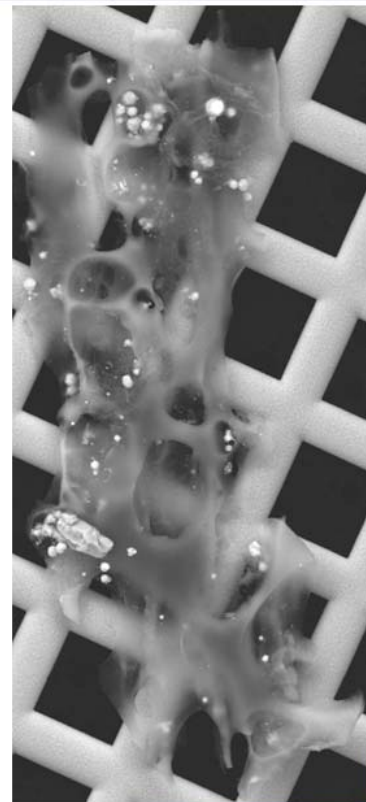
100 µm

Spore with mineral impressions
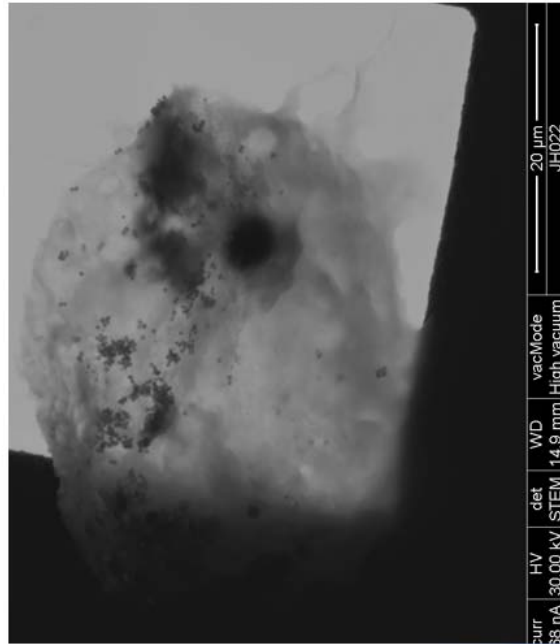
50 µm

Palynology cannot reach the same resolution as the goniatites and the preservation of the spores may not permit high resolution work.

Palynology cannot reach the same resolution as the goniatites and the preservation of the spores may not permit high resolution work.

Palynology cannot reach the same resolution as the goniatites and the preservation of the spores may not permit high resolution work.

Introduction Project Description Take away   Results   STEM   Py-GC   Biostrat.   Conclusions
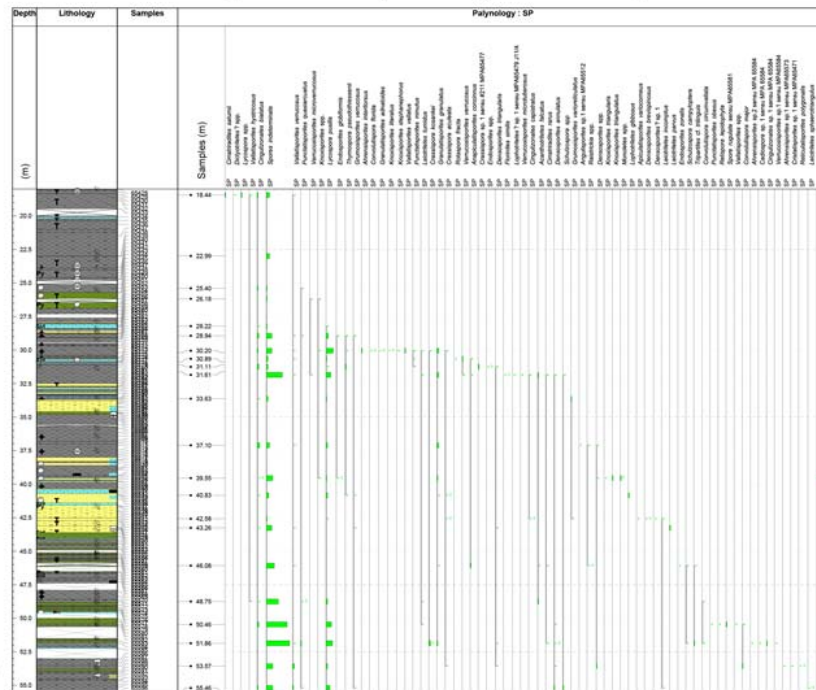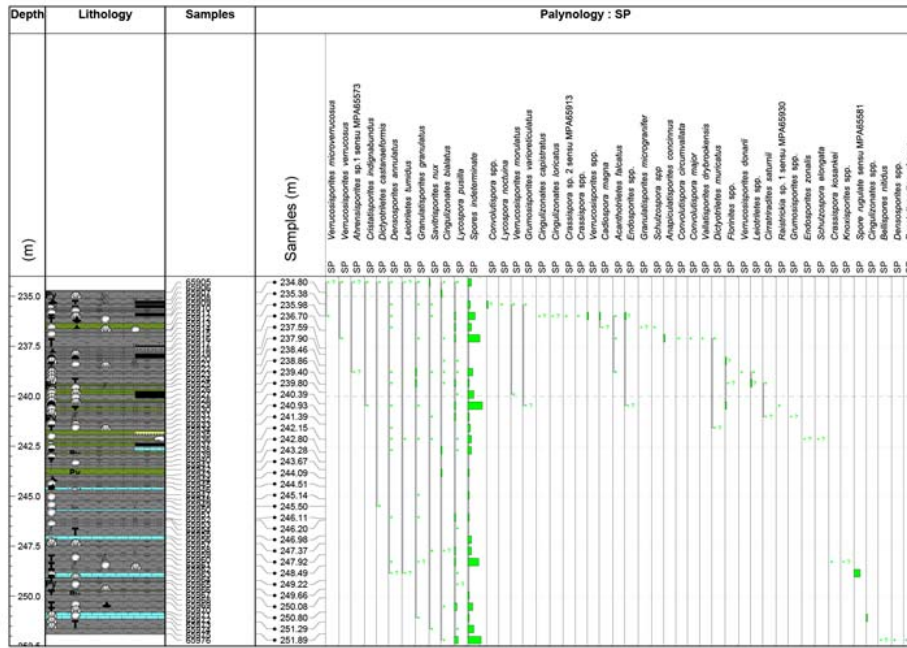
Conclusions

- **UK shale deposited** in fault bounded basins containing a mix of terrestrial and marine material. To define prospective horizons, a key parameter to consider will be the correct assessment of the origin of organic particles.

- **The development of a classification of the origin of AOM** in transmitted light has led to a limited understanding of what plant marine-derived AOM looks like.

- **STEM analysis** of isolated palynomorphs yields exciting taphonomical results but microstructures seem truly amorphous. The reactive surface of these particles is far greater than previously thought.

- **Spore biostratigraphy** will be crucial to resolve the finest stratigraphic changes between the different basins.

References

British Geological Survey holds most of the references listed below, and copies may be obtained via the library service subject to copyright legislation (contact libuser@bgs.ac.uk for details). The library catalogue is available at: https://envirolib.apps.nerc.ac.uk/olibcgi.

ANDREWS, I J. 2013. The Carboniferous Bowland Shale gas study: geology and resource estimation. *British Geological Survey for Department of Energy and Climate Change, London, UK.*

CLARKE, B.G. 1995. Pressure meters in geotechnical design *Blackie Academic and Professional.*

FISHER, K. & WARPINSKI, N. R. 2012. Hydraulic-Fracture-Height Growth: Real Data, *Society of Petroleum Engineers*, doi:10.2118/145949-PA.

HOBBS, P., OMAR, H. & WEST, L.J. 1997. A mini pressuremeter for measuring the tensile strength of weak rocks. International Society for Rock Mechanics (ISRM), Vol. 5, No. 1, Dec 1997, pp13-16.

HOUGH, E., CUSS, R.J., VANE, C.H., WATERS, C.N. & WU, X. 2015A. Onshore Carboniferous Basins- first review report. Commissioned report of the British Geological Survey No. CR/15/029.

HOUGH, E., CUSS, R.J., HASLAM, R.B., HOBBS, P.R.N., KEMP, S.J., KINGDON, A., MOSS-HAYES, V., RAINE, R., VANE, C.H., WATERS, C.N. & WOODS, M.A. 2015B. Onshore Carboniferous Basins- second review report. Commissioned report of the British Geological Survey No. CR/15/058.

JARVIE, D.M. 2012. Shale resource systems for oil and gas. In: J.A. Breyer (Editor), Giant resources for the 21st C. AAPG Memoir, pp. 89-119.

KAHRAMAN, S. 2001. Evaluation of simple methods for assessing the uniaxial compressive strength of rock *International Journal Rock Mechanical and Mining Sciences*, 38 (7) (2001), pp. 981–994

LOPATIN, N.V., ZUBAIRAEV, S.L., KOS, I.M., EMETS, T.P., ROMANOV, E.A. & MALCHIKHINA, O.V. 2003. Unconventional oil accumulations in the Jurassic Bazhenov black shale formation. Journal of Petroleum Geology, 26(2): 225-244.

MAIR, R.J. & WOOD, D.M. 1987. Pressuremeter testing – methods and interpretation. *Butterworth*.

MONAGHAN, AA & POULIQUEN, G. 2009. Clyde Regional Bedrock Model (Phase I) methodological report- BGS Project Document. British Geological Survey Internal Report IR/09/070.

SINGH, T.N., KAINTHOLA, A. & VENKATESH, A. 2012. Correlation between point load index and uniaxial compressive strength for different rock types. *Rock Mechanics and Rock Engineering*, 45 (2) (2012), pp. 259–264

SLOWAKIEWICZ, M., TUCKER, M., VANE, C.H., HARDING, R., COLLINS, A. & PANCOST, R.D. 2015. Shale-gas potential of the mid-Carboniferous Bowland-Hodder unit in the Cleveland basin (Yorkshire), Central Britain. Journal of Petroleum Geology, 38(1): 1-18

ULUSAY, R. & HUDSON, J A. 2007. The complete ISRM suggested methods for rock characterization, testing and monitoring: 1974-2006, Ankara, Turkey, Commission on Testing Methods, International Society of Rock Mechanics.